Stem Cell Research & Therapy

RESEARCH

Open Access

Clusterin-mediated polarization of M2 macrophages: a mechanism of temozolomide resistance in glioblastoma stem cells

Jianping Wen[1*], Xia Wu[1], Zhicheng Shu[1], Dongxu Wu[1], Zonghua Yin[1], Minglong Chen[1], Kun Luo[1], Kebo Liu[1], Yulong Shen[1], Yi Le[1] and Qingxia Shu[1*]

Abstract

Glioblastoma remains one of the most lethal malignancies, largely due to its resistance to standard chemotherapy such as temozolomide. This study investigates a novel resistance mechanism involving glioblastoma stem cells (GSCs) and the polarization of M2-type macrophages, mediated by the extracellular vesicle (EV)-based transfer of Clusterin. Using 6-week-old male CD34$^+$ humanized huHSC-(M-NSG) mice (NM-NSG-017) and glioblastoma cell lines (T98G and U251), we demonstrated that GSC-derived EVs enriched with Clusterin induce M2 macrophage polarization, thereby enhancing temozolomide resistance in glioblastoma cells. Single-cell and transcriptome sequencing revealed close interactions between GSCs and M2 macrophages, highlighting Clusterin as a key mediator. Our findings indicate that Clusterin-rich EVs from GSCs drive glioblastoma cell proliferation and resistance to temozolomide by modulating macrophage phenotypes. Targeting this pathway could potentially reverse resistance mechanisms, offering a promising therapeutic approach for glioblastoma. This study not only sheds light on a critical pathway underpinning glioblastoma resistance but also lays the groundwork for developing therapies targeting the tumor microenvironment. Our results suggest a paradigm shift in understanding glioblastoma resistance, emphasizing the therapeutic potential of disrupting EV-mediated communication in the tumor microenvironment.

Keywords Glioblastoma, Tumor stem cells, Macrophage polarization, Clusterin, Drug resistance

Introduction

Glioblastoma is one of the most common and aggressive central nervous system tumors, posing a significant threat to global health [1–3]. Classified into several subtypes by the World Health Organization (WHO), glioblastomas are notorious for their high malignancy and poor prognosis [4, 5]. The global incidence of glioblastoma continues to rise, making it a key focus of neuro-oncology research [6, 7]. Despite decades of medical advances, the five-year survival rate for glioblastoma remains below 5% [8]. This tumor is characterized by rapid growth, invasive behavior into surrounding brain tissue, and significant resistance to existing therapies [9, 10]. Its treatment is further complicated by considerable heterogeneity, as tumors within the same subtype can exhibit varying molecular features, growth patterns, and responses to therapy [11, 12]. These challenges highlight the need for a deeper understanding of glioblastoma biology and resistance mechanisms to develop innovative therapeutic approaches [13].

Temozolomide, an oral alkylating agent, is a standard treatment for high-grade glioblastoma [14–16]. It works by disrupting tumor cell DNA, inhibiting replication and division, and thereby slowing tumor growth [17].

*Correspondence:
Jianping Wen
wenjp2023@163.com
Qingxia Shu
2512868432@qq.com
[1] Department of Neurosurgery, Hunan University of Medicine General Hospital, No. 144, Jinxi South Road, Hecheng District, Huaihua 418000, Hunan Province, China

However, many patients eventually develop resistance to temozolomide, leading to treatment failure [18, 19]. Resistance mechanisms include enhanced DNA repair, immune suppression within the tumor microenvironment, and the involvement of tumor stem cells [20–22]. Tumor stem cells, known for their self-renewal and differentiation abilities, can survive chemotherapy and repopulate tumors, contributing to recurrence and progression [23–25]. Addressing temozolomide resistance is therefore an urgent research priority [26–28].

The tumor stem cell theory provides a new perspective on glioblastoma resistance [29]. Although they represent a small proportion of the tumor population, these cells exhibit robust tumorigenic potential and can resist therapeutic pressures, enabling tumor regrowth [30, 31]. The tumor microenvironment, comprising immune cells, vascular components, and extracellular matrix, offers critical support to tumor stem cells [32–34]. Among these components, macrophages play a pivotal role. Based on their functional states, macrophages are categorized as pro-inflammatory M1 or anti-inflammatory M2 [35]. M2 macrophages are particularly significant, as they promote tumor growth, suppress immune responses, and contribute to treatment resistance [36–38]. Understanding the interaction between tumor stem cells and macrophages, particularly the regulation of macrophage polarization, is crucial to addressing glioblastoma resistance [39, 40].

In this study, we used humanized $CD34^+$ huHSC-(M-NSG) mice (NM-NSG-017), a clinically relevant preclinical model, to replicate the human tumor microenvironment and explore resistance mechanisms in glioblastoma. This model, with its humanized immune system, is particularly suitable for studying interactions between tumor stem cells and macrophages, as well as their impact on temozolomide resistance. Moreover, using glioblastoma cell lines T98G and U251 ensures the clinical relevance of the findings, given their widely established use in glioblastoma research.

Although there is some understanding of the role of tumor stem cells in glioblastoma resistance, the precise regulation of this process, particularly how tumor stem cells influence the tumor microenvironment through secreted factors to promote resistance mechanisms, remains unclear [41–43]. Clusterin, a molecule involved in various biological processes, has increasingly drawn attention for its role in tumor development in recent years [44, 45]. However, its specific role in glioblastomas and its function in the interaction between tumor stem cells and the tumor microenvironment has not been fully elucidated [46, 47]. This study aims to explore how tumor stem cells mediate M2 macrophage polarization through the transfer of Clusterin via extracellular vesicles (EVs), thereby promoting resistance of glioblastomas to temozolomide. Through a comprehensive approach integrating single-cell sequencing, transcriptome sequencing, machine learning, and in vitro and in vivo experiments, this research unveils the critical role of Clusterin in regulating the tumor microenvironment, particularly in promoting M2 macrophage polarization. This discovery not only provides a new perspective on understanding the complex mechanisms of resistance in glioblastomas but also offers potential targets for developing novel treatment strategies targeting the tumor microenvironment, holding significant scientific and clinical implications.

Materials and methods

Preparation of samples for single-cell transcriptomics and high-throughput transcriptomics sequencing

Male C57BL/6 mice (strain: 219, Beijing Vital River Laboratory Animal Technology Co., Ltd., Beijing, China), aged six weeks, were reared under standard pathogen-free conditions. Before cell inoculation, the mice underwent acclimatization and health checks. A suspension of 5×10^6 GL261 cells (bio-105911, Beijing BioBow Biotechnology Co., Ltd., Beijing, China) in 0.2 mL was subcutaneously injected into the dorsal skin of the mice. Tumor growth was regularly measured using calipers, and the mice were humanely euthanized according to ethical guidelines when the experiment ended, or tumor volume reached 100 mm^3. Tumor and adjacent tissues were harvested for single-cell transcriptomics and high-throughput transcriptomics sequencing.

Single-cell sequencing data analysis

Tumor and adjacent non-tumor tissues from mouse models were selected for single-cell RNA sequencing (scRNA-seq). The analysis was conducted using the "Seurat" package in R software. Quality control steps were applied with filtering thresholds set as follows: nFeature_RNA > 500, nCount_RNA > 1000, nCount_RNA < 20,000, and percent.mt < 10. Canonical Correlation Analysis (CCA) was employed to eliminate batch effects, and data normalization was performed using the LogNormalize function. Principal Component Analysis (PCA) was subsequently conducted, and significant principal components were selected for t-SNE clustering analysis. The "SingleR" package was utilized to identify marker genes for each cell cluster, with the MouseRNAseqData function providing reference datasets for cell annotation. Statistical methods, including t-tests, were applied to compare the quantities and proportions of different cell types in cancerous and adjacent normal tissues. The results were visualized using the "ggplot2" package [48, 49].

Transcriptome sequencing analysis

Transcriptome sequencing was performed on tumor and adjacent tissues from three glioblastoma mouse models. Differential analysis was carried out using the "limma" package in R, with $|\log FC| > 1$ and $P < 0.05$ as selection criteria for differentially expressed genes (DEGs). Volcano plots were generated using the "ggplot2" package in R, and heatmaps of differential gene expression were created with the "heatmap" package [50, 51].

Differential gene function enrichment analysis

Candidate target genes were subjected to Gene Ontology (GO), KEGG, and Reactome enrichment analyses using the "ClusterProfiler" package in R, with a significance threshold of $P < 0.05$. GO analysis included Biological Process (BP), Molecular Function (MF), and Cellular Component (CC), providing insights into the cellular functions and signaling pathways influenced by these genes [52].

LASSO regression analysis

LASSO regression, a mathematical modeling technique, was used to establish quantitative relationships between dependent and independent variables. The "glmnet()" function in R Studio software was applied to load the candidate gene matrix. Under the condition $\alpha = 1$, an appropriate λ value was selected, and ten-fold cross-validation was conducted for internal validation to identify the optimal model [53].

Support vector machine-recursive feature elimination (SVM-RFE) analysis

The "e1071" and "caret" packages in R software were used to implement the Recursive Feature Elimination (RFE) algorithm for optimized gene selection. Gene expression data served as features, while clinical sample characteristics were treated as categorical variables. Support Vector Machine (SVM) with a linear kernel was utilized for prediction, and the RFE algorithm identified the best-performing gene features [54].

Construction of the random forest model

A random forest model was constructed using the "randomForest" function in R. Gene feature importance was assessed by calculating the "Mean Decrease Gini" in the decision tree. The top 30 genes were selected from a pool of 106 candidate genes based on this ranking [55].

Venn analysis

Venn analysis was conducted using the Draw Venn Diagram tool to obtain candidate genes [56].

Culturing glioblastoma cells and isolating tumor stem cells

Experiments utilized T98G (CRL-1690, ATCC, USA) and U251 (CC-Y5102, Shanghai Enzyme Research Biological Technology Co., Ltd., Shanghai, China) glioblastoma cell lines. Cells were cultured in high-glucose DMEM medium (11,965,118, Thermo Fisher Scientific, Waltham, MA, USA) supplemented with 10% fetal bovine serum (26,140,079, Thermo Fisher Scientific, Waltham, MA, USA) and 1% penicillin–streptomycin (100 U/mL penicillin and 100 μg/mL streptomycin). Once cells reached 80% confluency, tumor stem cells were isolated using flow cytometry (BD FACS Aria III, BD Biosciences, USA) with CD133-PE antibody (ab252128, Abcam, UK) and CD15-FITC antibody (ab18272, Abcam, UK).

Isolation and characterization of EVs

EVs were isolated from sorted tumor stem cells using a gradient centrifugation method with an ultracentrifuge (Optima XPN-100, Beckman Coulter, USA). Initially, the cell culture supernatant was centrifuged at 5000 g for 10 min to remove cell debris. The supernatant was then subjected to ultracentrifugation at 100,000 g to collect EVs. The morphology of the EVs was analyzed using transmission electron microscopy (JEM-1400Flash, JEOL, Japan), while their size distribution was determined using a nanoparticle tracking analysis system (NTA, NanoSight NS300, Malvern Panalytical, UK).

Diluted samples (1:20) were loaded onto Formvar-coated copper grids (5 μL). Grids were incubated for 20 min, followed by fixation with 2% paraformaldehyde for 5 min. The samples were washed with PBS, then fixed with 1% glutaraldehyde for 5 min, rinsed with Milli-Q water, and stained with 1.5% uranyl acetate for 4 min. Images were captured using a Gatan OneView 4 K camera operating at 200 kV, installed on a Jem-2100Plus (Jeol) microscope.

Dil staining

Before Dil staining, EVs were co-incubated with THP-1 cells (CC-Y1519, Shanghai Enzyme Research Biotechnology Co., Ltd., Shanghai, China). THP-1 cells were cultured in RPMI 1640 medium (L210KJ, Shanghai Enzyme Research Biotechnology Co., Ltd., Shanghai, China) supplemented with 10% fetal bovine serum and 1% penicillin–streptomycin at 37 °C in 5% CO_2. Differentiation of THP-1 cells into macrophages was induced with 100 nM PMA (Sigma-Aldrich, USA) for 48 h. After 24 h of co-incubation, a Dil fluorescent tracer (Thermo Fisher

Scientific, USA) was added to label EVs. A 1 mg/mL Dil solution was incubated with the EV-THP-1 cell culture at 37 °C for 30 min, followed by PBS washes to remove unbound dye. Microscopic observation and image acquisition were conducted using confocal laser scanning microscopy (Leica TCS SP8, Wetzlar, Germany). The experiment was repeated three times, with results validated through statistical analysis [57].

RT-qPCR

Cellular total RNA was extracted using Trizol reagent (15,596,026, Invitrogen, Carlsbad, CA, USA), and the concentration and purity of the extracted total RNA were assessed using a Nanodrop 2000 spectrophotometer (1011U, Nanodrop, USA). The RNA was reverse transcribed into cDNA following the instructions of the PrimeScript RT reagent Kit (RR047A, Takara, Japan) under the conditions of 42 °C for 30–50 min, followed by 85 °C for 5 s. Subsequently, qRT-PCR analysis was performed using the Fast SYBR Green PCR kit (RR820A, Takara, Japan) on an ABI PRISM 7300 RT-PCR system (Applied Biosystems). The reaction conditions included an initial denaturation at 95 °C for 5 min, followed by 40 cycles of denaturation at 95 °C for 30 s, annealing at 57 °C for 30 s, and extension at 72 °C for 30 s. Three technical replicates were set for each sample. GAPDH served as the internal control, and the relative gene expression was analyzed using the $2^{-\Delta\Delta Ct}$ method, where ΔΔCt = (average Ct value of the target gene in the experimental group—average Ct value of the housekeeping gene in the experimental group)—(average Ct value of the target gene in the control group—average Ct value of the housekeeping gene in the control group) [58]. Each experiment was replicated three times. Primer sequences are listed in Table S1.

Western blot

Total protein was extracted using RIPA lysis buffer (P0013B, Beyotime, Shanghai, China) supplemented with 1% phenylmethanesulfonyl fluoride (PMSF), following the manufacturer's protocol. Protein concentration was quantified with a BCA protein assay kit (P0011, Beyotime, Shanghai, China) and adjusted to 1 μg/μL. Samples were denatured at 100 °C for 10 min and stored at − 80 °C.

Proteins were separated on 8–12% SDS-PAGE gels at a constant voltage of 80–120 V for 2 h and transferred to PVDF membranes (1,620,177, Bio-Rad, USA) using a constant current of 250 mA for 90 min. Membranes were blocked in 1xTBST containing 5% skimmed milk at room temperature for 1 h, followed by incubation with primary antibodies overnight at 4 °C (antibody details in Table S2). Secondary antibody incubation with HRP-conjugated goat anti-rabbit or anti-mouse IgG (1:5000) was performed for 1 h. Protein bands were visualized using ECL reagents (1,705,062, Bio-Rad, USA) on an Image Quant LAS 4000C system (GE Healthcare, USA). Band intensities were quantified by comparing target proteins to β-actin controls, with experiments repeated three times [59].

Immunofluorescence staining

Cells were rinsed with cold PBS and fixed with 4% paraformaldehyde for 15–30 min. Subsequently, cells were permeabilized with 0.1% Triton (L885651, Macklin, Shanghai, China) for 15 min to penetrate the cell membrane. After two washes with PBS, cells were incubated in PBS containing 15% FBS overnight at 4 °C for 4 min. Clusterin (ab69644, diluted 1:200, Abcam, USA), CD206 (MA5-16,871, diluted 1:200, ThermoFisher), CD163 (ab182422, 1:200, abcam, USA), CD80 (ab254579, 1:200, abcam, USA), CD86 (ab239075, 1:100, abcam, USA) were added and incubated at 37 °C for 60 min. PBS wash was carried out for 5 min, repeated three times. Cells were then incubated with goat anti-rabbit IgG (H + L) (65–6111, ThermoFisher) and donkey anti-mouse IgG (H + L) (A21202, ThermoFisher) for 1 h at 37 °C, followed by 60 min avoiding light, and washed with PBS for 3 min, repeated three times. DAPI staining was performed for 10 min, followed by three washes with PBS. Finally, samples were mounted with a 20 μL mounting medium and immediately observed under a fluorescence microscope [60].

Construction and validation of temozolomide-resistant glioblastoma cell line

A temozolomide-resistant cell model was established using the T98G glioblastoma cell line. Initially, cells were seeded in 6-well plates coated with cell adhesion protein (176,740, ThermoFisher) and cultured for six months with increasing concentrations of temozolomide (PHR1437, Sigma-Aldrich, USA) ranging from 5 to 200 μM. The concentration of temozolomide was increased by 32.5 μM every four weeks. Once cells were able to proliferate at 200 μM temozolomide, the stable resistant cell line was established. The resistance phenotype was maintained by culturing cells in 200 μM temozolomide. At each concentration, cells were passaged when their survival density reached 80–90%. The culture medium containing temozolomide was replaced every 2–3 days [61].

Constructing lentivirus

Lentivirus packaging services were provided by Sangon Biotech (Shanghai, China). The pHAGE-puro series plasmid, along with auxiliary plasmids pSPAX2 and pMD2.G, and the pSuper-retro-puro series plasmid with auxiliary

plasmids gag/pol and VSVG were co-transfected into 293 T cells (CRL-3216, ATCC, USA). Following 48 h of cell culture, the supernatant was collected, filtered through a 0.45 μm filter, and the concentrated virus was harvested by centrifugation. After 72 h, the supernatant was collected, concentrated by centrifugation, and a mixture of the two viruses was prepared and titrated. The lentiviral silencing sequences are shown in Table S3, and the silencing efficiency was validated in the T98G cell line, as illustrated in Fig. S1. Subsequently, the sequence with the most favorable silencing effect (Sh-Clusterin-2) was selected for experimentation [62].

For cell transfection, the working titer of the lentivirus was maintained at 5×10^6 TU/mL, with a consistent incubation time of 48 h.

Co-culture of T98GR and THP-1 cells

Both cell types and appropriate media were prepared for co-culture. A Transwell chamber with a pore size of 0.4 μm was used, placing T98GR cells in the upper chamber and THP-1 cells in the lower chamber. Both cell types were seeded at a 1:1 ratio. THP-1 cells were seeded on the bottom of the culture dish below the Transwell insert, and T98GR cells were seeded on the membrane of the Transwell insert. Co-culture was performed with regular medium changes.

MTT assay

The MTT assay is utilized to analyze cell viability and determine the 50% inhibitory concentration (IC50). A total of 0.3×10^4 cells were seeded in each well of a 96-well plate and incubated overnight. Subsequently, the cells were treated with various doses of MPA for 48 h. Following this, 10 μL of MTT solution (5 mg/mL in PBS, 11,465,007,001, Merck) was added to each well and incubated at 37 degrees Celsius for 4 h. The formazan crystals formed were then dissolved in 150 μL of dimethyl sulfoxide (DMSO; Sigma-Aldrich, St. Louis, Missouri, USA). Absorbance was measured at a wavelength of 550 nm [63].

CCK-8

Cells in a state of good growth were seeded in a 96-well plate at a density of 8×10^3 cells per well and incubated in a culture chamber. At specific time points during the culture period (24 h, 48 h, and 72 h), 10 μL of CCK-8 solution (96,992, Sigma-Aldrich, USA) was added to each well. After incubation at 37 ℃ in a humidified incubator for 1 h, the absorbance of each sample was measured at 450 nm using the Epoch microplate spectrophotometer (Bio-Tek, Winooski, VT, USA). Each group was set up with 6 replicates, and the experiment was repeated 3 times [64, 65].

Transwell experiment

Following different treatments for 24 h, a Transwell invasion assay was conducted. The Transwell inserts with an 8 μm pore size were coated with 50 μL of basement membrane matrix (354,234, BD Biosciences, USA) and incubated at 37 °C for 30 min to allow gel solidification. The inserts were then rinsed with culture medium without FBS, and the cells were diluted to a concentration of 2.5×10^4 cells/mL in an FBS-free medium. Subsequently, 100 μL of the cell suspension was added to each insert chamber, while 500 μL of medium containing 10% FBS was added to the lower chamber. After 24 h, the inserts were removed, the cells in the upper chamber were removed with a cotton swab, and the remaining cells were fixed with 4% PFA at room temperature for 30 min. Following fixation, cells were stained with 0.1% crystal violet for 30 min. Five random areas were selected, images were captured under an inverted microscope (IXplore Pro, Olympus, Japan), cell counting was performed, and the experiment was repeated three times. For the cell migration assay, no basement membrane matrix was added, while the remaining steps were identical to the invasion assay [66].

Experimental tumor transplantation in mice

Drawing upon the literature [67] and following the 3Rs principle (replace, reduce, refine), twenty-four $CD34^+$ healthy 6-week-old humanized huHSC-(M-NSG) mice (NM-NSG-017) were obtained from Shanghai Southern Model Biotechnology Co., Ltd. (Shanghai, China) and housed in SPF-grade animal facilities at a humidity of 60–65% and a temperature of 22–25 ℃. The mice were acclimated for one week before the experiment, and their health status was assessed prior to the experiment. All animal procedures were approved by the Institutional Animal Care and Use Committee.

Prior to tumor cell injection, mice were anesthetized with intraperitoneal administration of 1–2% isoflurane (in oxygen) using a precision vaporizer to ensure adequate sedation and minimize discomfort. Anesthesia depth was monitored based on the absence of a pedal withdrawal reflex. Following anesthesia induction, the mice were placed in a sterile environment for the subcutaneous injection of tumor cells. Post-injection, the mice were monitored until they regained full consciousness. Minor weight loss and transient lethargy after EV injections were observed but resolved within 24 h; no unexpected adverse events occurred. The mice were randomly divided into four groups, each consisting of six mice. The groups were designated as follows:

(1) PBS Group: T98G cells were subcutaneously injected, followed by daily oral administration of

50 mg/kg temozolomide and intravenous injection of PBS every three days.

(2) EV Group: T98G cells were subcutaneously injected, followed by daily oral administration of 50 mg/kg temozolomide and intravesicular treatment every three days.

(3) sh-NC + EV Group: Temozolomide-resistant T98G cells were subcutaneously injected, followed by intravenous injection of EVs collected from tumor stem cells transfected with sh-NC after two weeks. Subsequently, daily oral administration of 50 mg/kg temozolomide was performed, along with EV treatment administered intravenously every three days.

(4) sh-Clusterin-EV Group: Temozolomide-resistant T98G cells were subcutaneously injected, followed by intravenous injection of EVs collected from tumor stem cells transfected with sh-Clusterin after two weeks. Subsequently, daily oral administration of 50 mg/kg temozolomide was performed, along with EV treatment administered intravenously every three days.

Specifically, drug-resistant T98G cells (5×10^6/0.2 mL) were injected subcutaneously into the back of $Rag1^{-/-}$ mice. The width (W) and length (L) of the tumors in nude mice of each group were measured weekly using a caliper to monitor tumor growth. The tumor volume (V) was calculated using the formula $V=(W^2\times L)/2$. When the tumor volume reached approximately 100 mm^3, EVs isolated from tumor stem cells (200 μg per dose) were administered via tail vein injection every three days. For the PBS group, an equivalent volume of PBS was injected via the tail vein every three days as a control. After 40 days, mice were euthanized following ethical guidelines. Prior to euthanasia, animals were anesthetized using 5% isoflurane in oxygen. Cervical dislocation was then performed by placing the mouse on a firm surface, gently restraining the head with one hand, and quickly pulling the tail downward with the other hand to dislocate the cervical spine, ensuring a rapid and painless process. Tumor tissues were then collected.

Tumors were dissected and weighed, with the tissue divided into two portions: one was fixed in 4% paraformaldehyde for staining, and the other was frozen in liquid nitrogen and stored at −80 °C for subsequent experimental analysis [68, 69].

Hematoxylin and eosin staining

Tissue sections were first stained in a container containing a solution of hematoxylin (Sigma-Aldrich, USA) for 5 min to stain the cell nuclei. Subsequently, rapid destaining was performed in a container containing 1% acidic alcohol, followed by staining in eosin solution (Sigma-Aldrich, USA) for 3 min to stain the cytoplasm and intercellular matrix. Post-staining, the sections were dehydrated twice in 95% alcohol, cleared, and mounted with neutral resin. Morphological images were observed and captured using an optical microscope (Leica Microsystems, Germany). Image analysis was conducted using ImageJ software (NIH, USA, version 1.52a) for quantitative assessment of nuclear and cytoplasmic features. All procedures were conducted at room temperature, ensuring rinsing of excess dye with distilled water after each step. At least three sections were prepared under each experimental condition and the procedures were repeated three times to ensure result reproducibility.

Immunohistochemical staining

The paraffin embedding process began by cooling molten paraffin on ice or in a 4 °C refrigerator before embedding tissue slices. Paraffin-embedded slices were air-dried overnight and baked at 60 °C for 20 min. The slices were immersed in xylene twice for 10 min each, followed by dehydration in absolute alcohol twice for 5 min. Hydration was performed sequentially in 95 and 70% alcohol for 10 min each, followed by a 5 min wash in distilled water. Antigen retrieval was conducted by microwaving slices in citrate buffer (pH 6.0) at high power for 1 min and 20 s, then cooling to room temperature and washing with PBS three times for 3 min each. Endogenous enzymes were inactivated with 3% H_2O_2 for 10 min at room temperature, followed by PBS washes.

Slides were blocked with normal goat serum (E510009, GenePharma) at room temperature for 20 min, then incubated overnight at 4 °C with primary antibodies for clusterin (ab92548), CD206 (ab64693), and CD80 (ab134120) (Abcam). After washing, slides were treated with biotinylated goat anti-mouse/rabbit IgG polymer (pv6000/pv9000, Zhongsheng Golden Bridge) for 30 min and stained using a DAB chromogenic reagent kit (ZLI-9018, Zhongsheng Golden Bridge). Staining was observed and photographed under a microscope [70].

For the analysis of antibody-positive areas in IHC images, TIFF image files were opened in ImageJ and converted to 8-bit grayscale images. Representative samples of minimum, maximum, and intermediate staining intensities were displayed to establish optimal threshold values. The threshold was determined to accurately reflect staining patterns under all experimental conditions and kept consistent across all images in the cohort. Black-and-white images of selected regions of interest were then generated, and the "Analyze Particles" function was used to quantify the percentage of stained area. At least six views from each sample region were analyzed and averaged [71].

Statistical analysis methods

All data were processed using GraphPad Prism 8.0. Continuous data were presented as mean ± standard deviation (Mean ± SD). Multiple statistical analysis methods were employed in this study to process and interpret data effectively. The comparison between the two groups was conducted using an unpaired t-test, while the comparison among multiple groups was performed utilizing one-way analysis of variance (ANOVA). Homogeneity of variance was assessed using the Levene test. If the variances were homogeneous, pairwise comparisons were conducted using Dunnett's t and LSD-t tests. In cases of inhomogeneous variances, Dunnett's T3 test was applied. Spearman or Pearson analysis was employed to examine the correlation between genes and the content of immune cells. A significance level of $P < 0.05$ indicated statistical significance in the comparison between two groups.

This study has been conducted and reported in accordance with the ARRIVE guidelines 2.0

Results

Analysis of highly variable genes and reliable PCA in glioblastoma tissues using scRNA-seq

We utilized the "Seurat" package in R software to analyze scRNA-seq data from glioblastoma tissues. Following quality control and normalization of the scRNA-seq data, we obtained the distribution of cell RNA, as shown in Fig. 1A. We then calculated the S.Score and G2M.Score of the data (Fig. 1B) and subsequently selected the top 2000 highly variable genes for downstream analysis (Fig. 1C). These results demonstrate the presence of numerous highly variable genes in glioblastoma tissues.

Subsequently, we performed PCA to reduce the dimensions of the aforementioned 2000 genes. Through PCA reduction, we identified the most significant

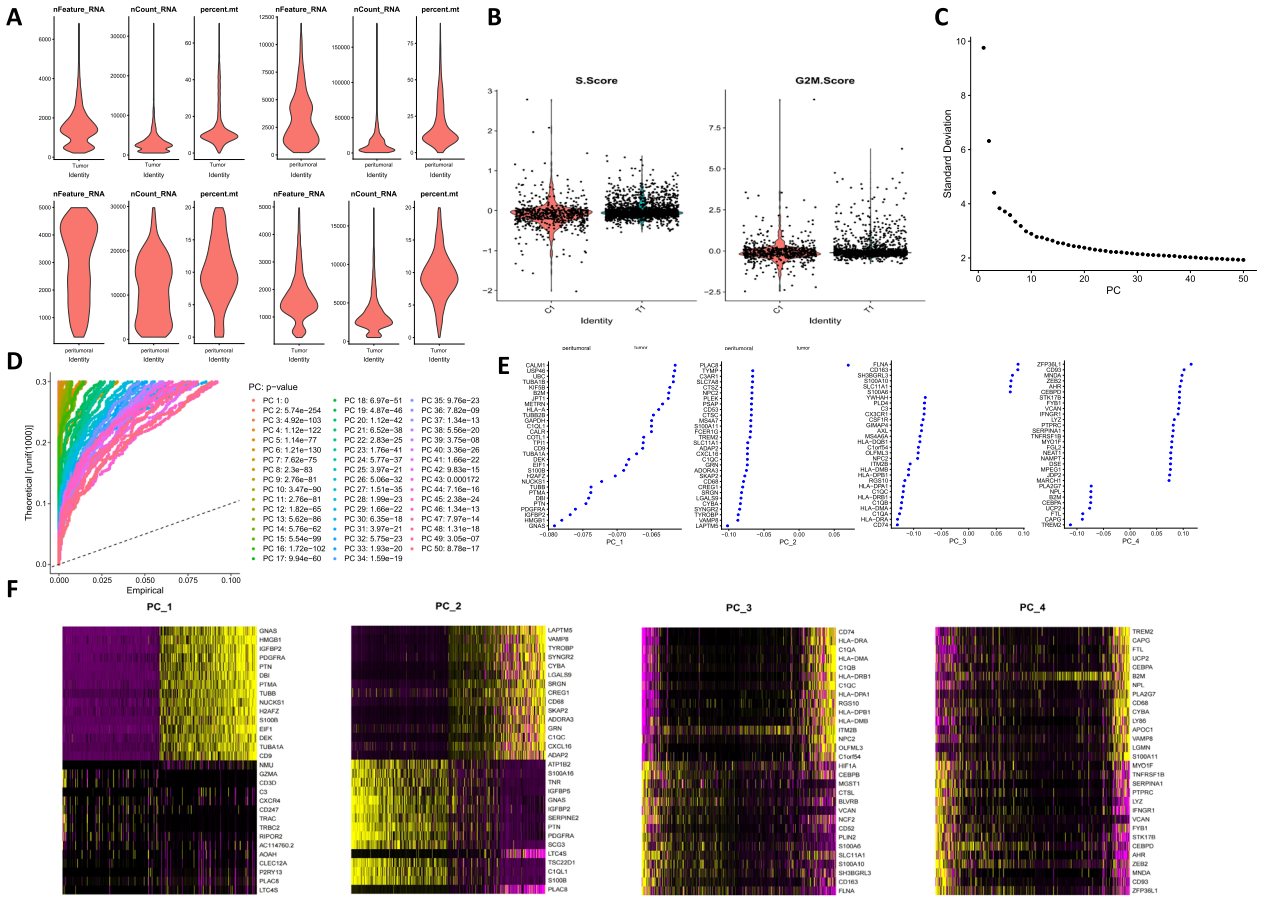

Fig. 1 Quality Control, Filtering, and PCA of scRNA-seq Data. Note: **A** Quality control of each cell in scRNA-seq data, with three scatterplots displaying the quantities of nFeature_RNA, nCount_RNA, and percent.mt in each cell; **B** Computation of S.Score and G2M.Score for scRNA-seq data; **C** Results of dimensionality reduction analysis, where each point represents a single cell; **D** p-values of the top 50 principal components (PCs) obtained from PCA analysis of cells from different sample sources; **E** Dot plot showing the expression levels of feature genes in the top 4 PCs of PCA analysis; **F** Heatmap illustrating the expression levels of feature genes in the top 4 PCs of PCA analysis, with yellow indicating upregulation and purple indicating downregulation; n(peritumoral) = 1, n(tumor) = 1

PCs with abundant low p-values. Utilizing the JackStrawPlot function for visualization, we compared the p-value distributions of each PC relative to the mean distribution. The significant PCs typically exhibited very low p-values (indicated by solid lines above the dashed line), effectively capturing the information contained within the highly variable genes selected earlier. In total, 50 PCs were obtained from the PCA analysis (Fig. 1D). Heatmaps and bubble plots showing the expression levels of characteristic genes for the top 4 PCs are displayed in Figs. 1E, F. These findings suggest that the PCA results are reliable and can be utilized for subsequent cell clustering analyses.

Crosstalk analysis between tumor stem cells and M2-type macrophages in glioblastoma

To further characterize cell types, we initially utilized the Find Clusters function to determine the optimal number of clusters (Fig. 2A). Subsequently, all cells were clustered into five cell clusters using t-SNE analysis (Fig. 2B). Following this, marker genes were selected, and we employed the Bioconductor/R package "SingleR" to annotate the five cell clusters, resulting in

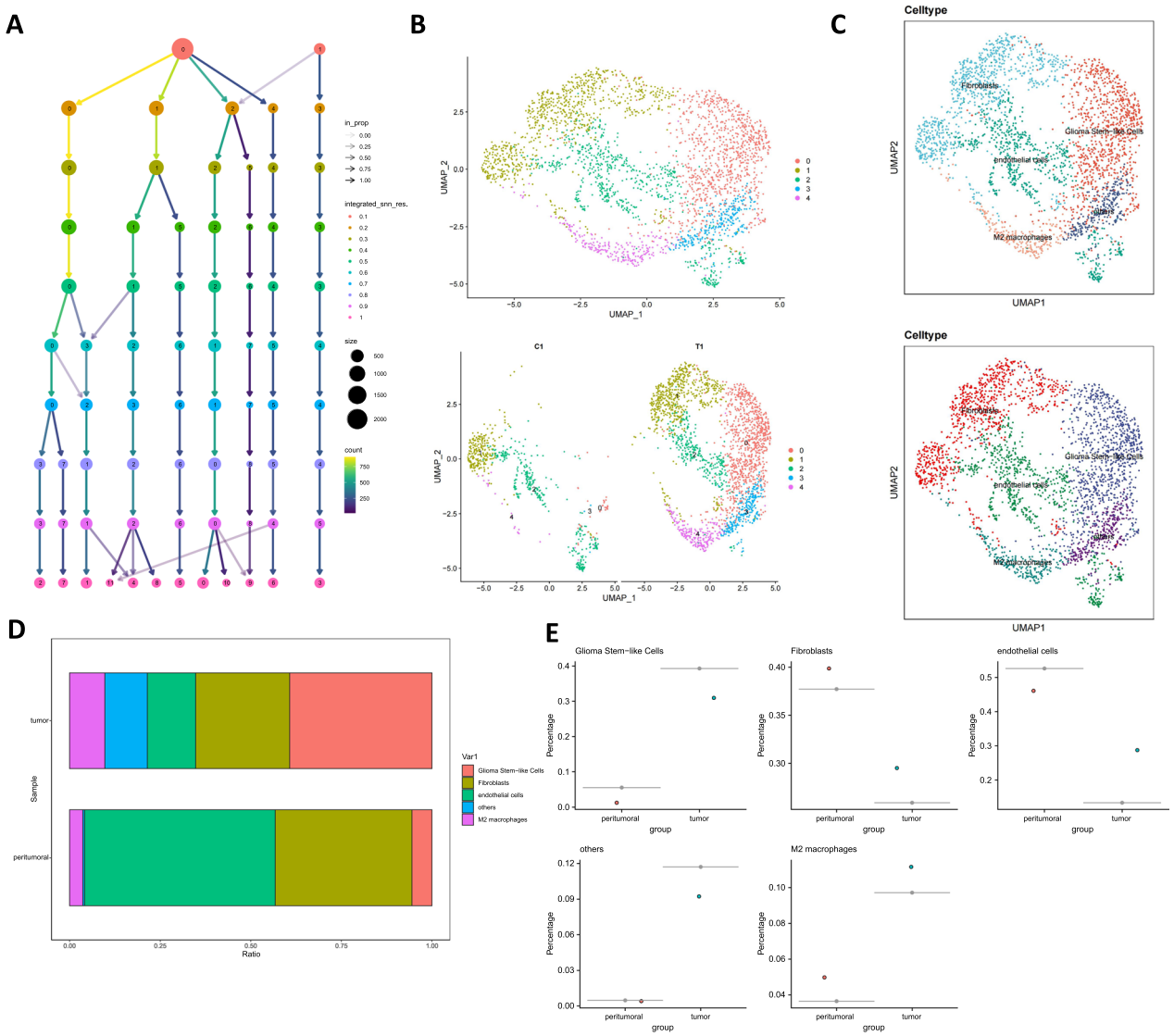

Fig. 2 scRNA-seq Cell Clustering Analysis. Note: **A** The Find Clusters function selects the optimal number of clusters; **B** t-SNE clustering analysis divides cells into 5 cell clusters and illustrates the distribution of these 5 clusters in two groups; **C** Single R annotates the 5 cell clusters as 4 cell types; **D** The proportion of the 5 cell types in each sample; **E** Comparison of the 5 cell types across different samples; n(peritumoral) = 1, n(tumor) = 1

the identification of four cell types: Glioblastoma Stem-like Cells, Fibroblasts, endothelial cells, and M2 macrophages (Fig. 2C).

Moreover, the proportions of these four cell types in two samples were visualized (Fig. 2D, E), demonstrating an increased proportion of M2 macrophages and Glioblastoma Stem-like Cells in tumor tissues. Studies have indicated that M2-type macrophages exacerbate the malignant progression of glioblastoma by promoting the proliferation of tumor stem cells and maintaining their stem cell status. Conversely, tumor stem cells can induce the polarization of surrounding macrophages into the M2 type by secreting specific signaling molecules such as VEGF and EGF, thus creating a microenvironment that promotes tumor growth and immune evasion [72]. Based on this, further investigation was conducted to explore the regulatory mechanisms between tumor stem cells and M2-type macrophages in glioblastoma.

The crucial role and potential mechanisms of clusterin in glioblastoma development

To delve deeper into the core genes influencing glioblastoma, transcriptome sequencing analysis was conducted on tumor tissues of mice with glioblastoma. The analysis of DEGs yielded a total of 221 genes (Fig. 3A). Functional enrichment analysis was then performed on these DEGs, revealing that they are mainly involved in regulating mechanisms such as negative chemotaxis, neuron fate determination, and RNA polymerase II cis-regulatory region sequence-specific DNA binding according to GO enrichment analysis. Moreover, Kyoto Encyclopedia of Genes and Genomes (KEGG) enrichment analysis indicated their involvement in Glycolysis/Gluconeogenesis, Synthesis and degradation of ketone bodies, and Steroid biosynthesis mechanisms. Additionally, Reactome enrichment analysis showed that the DEGs are mainly associated with the regulation of MET activates PTK2 signaling, Extracellular matrix organization, and MET promotes cell motility (Fig. 3B–D).

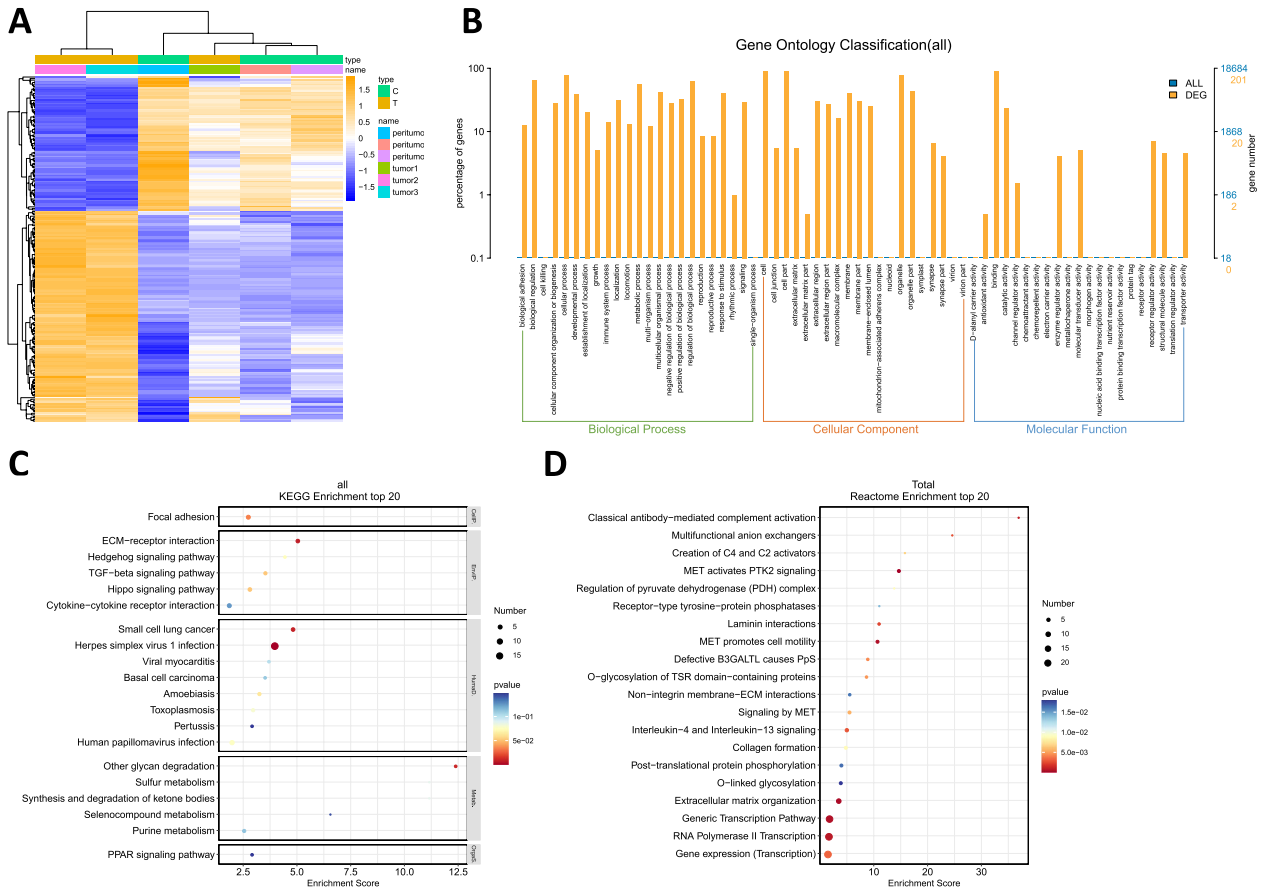

Fig. 3 Transcriptomic Analysis of Glioblastoma. Note: **A** Transcriptomic sequencing analysis of glioblastoma tissues in mice, presenting differential expression heatmap and volcano plot; **B** Gene Ontology enrichment analysis of DEGs; **C** Kyoto Encyclopedia of Genes and Genomes (KEGG) enrichment analysis of DEGs; **D** Reactome enrichment analysis of DEGs; n(peritumoral) = 3, n(tumor) = 3

Subsequently, essential DEGs involved in glioblastoma initiation and progression were identified by subjecting the 221 candidate DEGs to LASSO regression analysis. Utilizing the LASSO algorithm with the L1 criterion for model construction, the variations of regression coefficients under the L1 criterion are shown in Fig. 4A. A parameter $\alpha = 1$ was selected, and a tenfold cross-validation was employed for internal model validation. Two candidate DEGs were identified as potential biomarkers influencing glioblastoma progression.

To address potential data bias arising from the imbalance between norperitumoral and tumor tissues in the dataset, the SVM-RFE algorithm was applied, as depicted in Fig. 4B. Through this algorithm, the optimal gene feature combination was selected from the 221 candidate DEGs. Subsequently, a random forest tree model was constructed using the randomForest function to screen the top 30 genes ranked by Mean Decrease Gini (Fig. 4C). Through Venn analysis, Clusterin was identified as a gene shared by all three algorithms (Fig. 4D). Analysis of the sequencing data revealed a significant upregulation of Clusterin mRNA in tumor tissues compared to the control group (Fig. 4E).

Furthermore, combining single-cell sequencing data illustrated the distribution of Clusterin in glioblastoma tissues (Fig. 5A). Moreover, data from The Human Protein Atlas website indicated the presence of Clusterin in brain glioblastoma tissues (Fig. 5B). Additionally, a Protein–Protein Interaction (PPI) regulatory network was constructed using the GeneMania website, revealing interactive relationships between Clusterin and tumor stem cell marker genes, as well as M2 macrophage marker genes (Fig. 5C, D). Therefore, Clusterin may participate in the interaction between tumor stem cells and M2 macrophages during the development of glioblastoma.

Promotion of M2 macrophage polarization by tumor stem cell-derived EVs

Through the aforementioned bioinformatics analyses, we have elucidated the significant role of Clusterin in glioblastoma, with its crucial mechanism likely being the induction of M2 macrophage polarization. To delve deeper into the mechanisms of temozolomide resistance in glioblastoma cells, initial experimental validation was conducted in vitro. Tumor stem cells were successfully isolated from T98G and U251 glioblastoma cell lines. By utilizing flow cytometry combined with CD133-PE

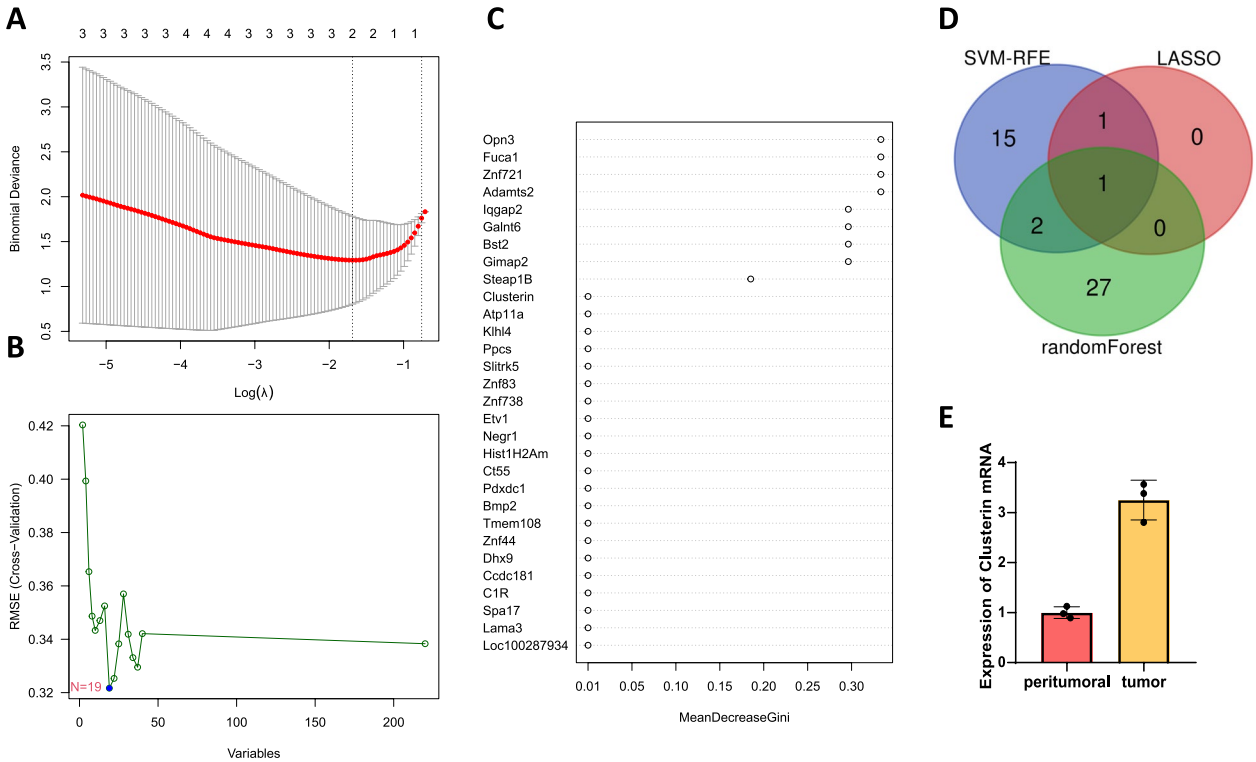

Fig. 4 Core Genes Screening for Glioblastoma. Note: **A** Graph depicting the selection process of the cross-validation parameter λ; **B** Line graph of the tenfold cross-validation for feature selection using the VM-RFE algorithm; **C** Calculation of Mean Decrease Gini for DEGs; **D** Venn analysis for selecting common feature genes obtained from LASSO, SVM-RFE, and randomForest; **E** Comparison of Clusterin mRNA expression in tumor tissues versus the control group; *, indicating a significance level of $P < 0.05$ compared to the control group; n(peritumoral) = 3, n(tumor) = 3

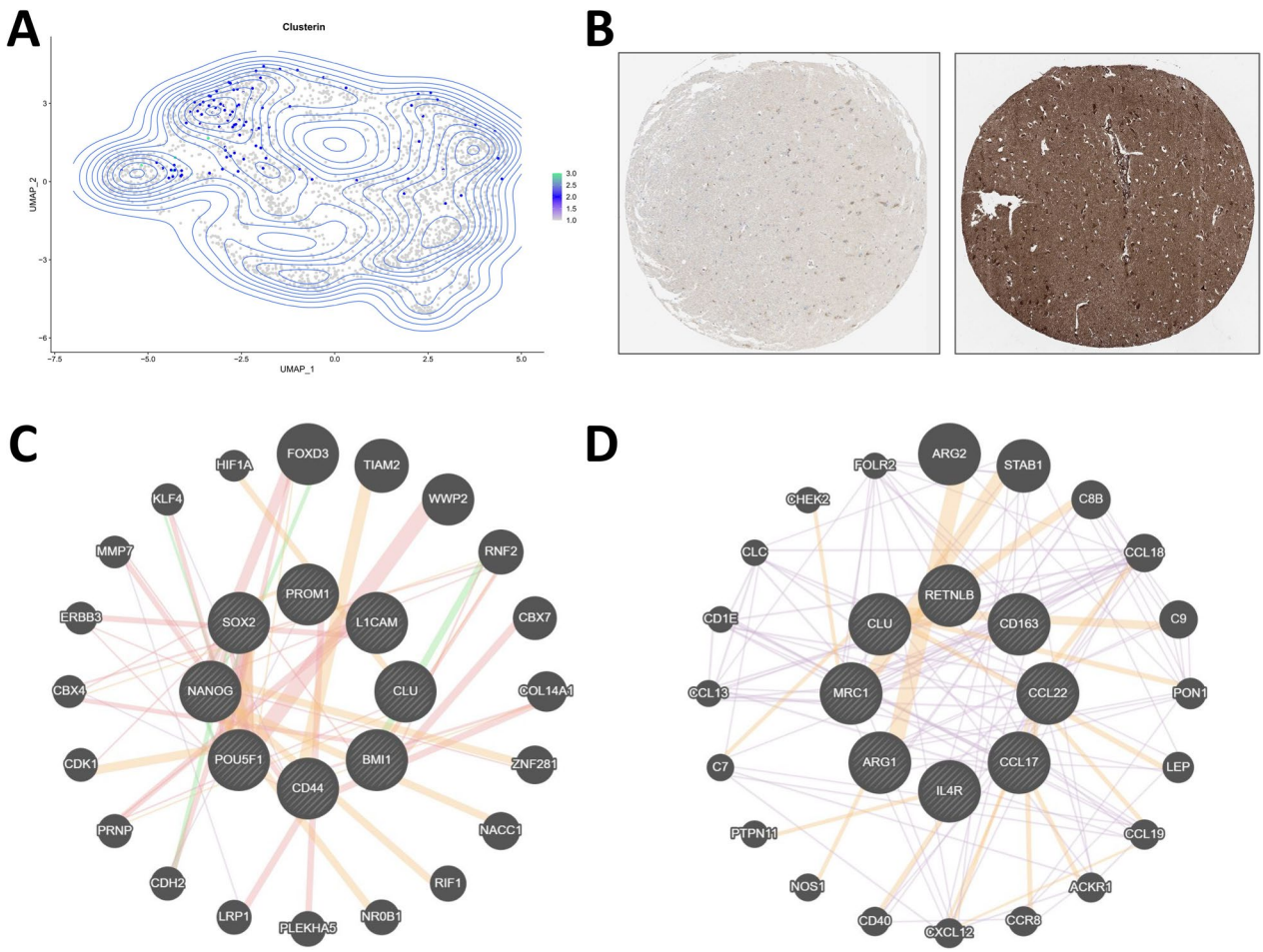

Fig. 5 Exploration of Clusterin Function. Note: **A** Expression area map of Clusterin in single-cell sequencing profiles, n(C) = 1, n(T) = 1; **B** Protein expression map of Clusterin in THE HUMAN PROTEIN ATLAS website; **C** Interaction network of Clusterin with tumor stem cell marker genes; **D** Interaction network of Clusterin with M2 macrophage marker genes

and CD15-FITC antibodies, cells expressing these markers were identified and separated to ensure the purity and specificity of the tumor stem cells (Fig. 6A). Subsequently, EVs were isolated from these tumor stem cells. The presence of EVs was confirmed and their size distribution quantified through ultracentrifugation and NTA (Fig. 6B). Transmission electron microscopy observation revealed that these EVs exhibited typical membrane structures, with diameters predominantly ranging from 30 to 150 nm (Fig. 6C). Western blot experiments showed high expression of extracellular vesicle markers TSG101 and CD63 in T98G-EV and U251-EV, while the negative marker GM130 was not expressed in T98G-EV and U251-EV (Fig. 6D).

Subsequently, these EVs were co-cultured with THP-1 monocytes induced to differentiate into macrophages to investigate the impact of EVs on macrophage polarization. To induce THP-1 differentiation into macrophages, all cell groups were treated with PMA. Dil-stained EVs were clearly visible under fluorescence microscopy, confirming their successful interaction with macrophages (Fig. 6E). PCR-qPCR and Western blot analysis revealed a significant increase in the expression of M2 markers CD206, CD163 and a relative decrease in M1 markers CD80, and CD86 in co-cultured macrophages compared to untreated macrophages (Fig. 6F). This result indicates that EVs derived from tumor stem cells can promote macrophage polarization towards the M2 phenotype. Additionally, immunofluorescence results observed Clusterin fluorescence positivity in the cytoplasm (Fig. 6G), and Western blot analysis confirmed the enrichment of Clusterin protein in EVs, suggesting its potential role in mediating macrophage polarization (Fig. 6H).

M2 macrophages, a type of immune cell, are believed to play a crucial role in tumor growth, proliferation, and immune function due to their polarization status. In the tumor microenvironment, M2 macrophages are associated with tumor-associated macrophages (TAMs),

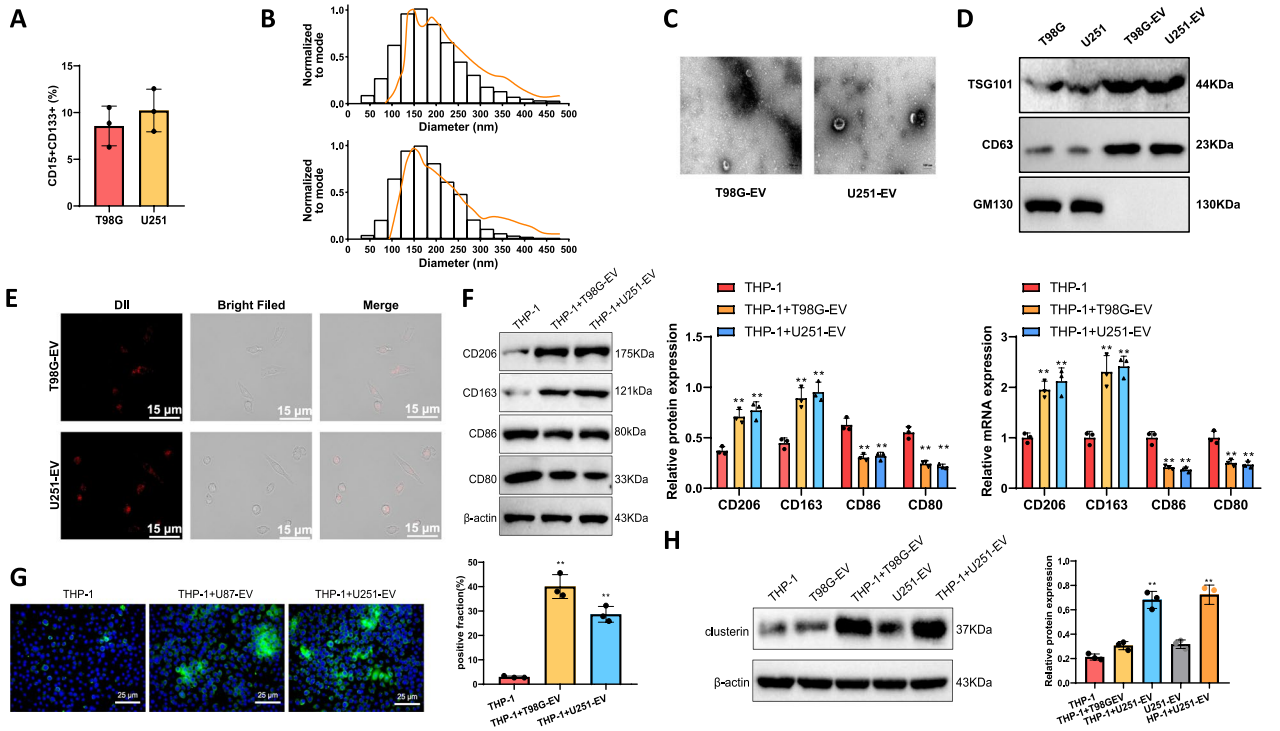

Fig. 6 The Role of Exosomes Derived from Tumor Stem Cells in M2 Macrophage Polarization. Note: **A** Flow cytometry was used to detect and isolate $CD133^{+}CD15^{+}$ cells from T98G and U251 cell lines. **B** Size distribution graph of exosomes obtained by ultracentrifugation and analyzed using a nanoparticle tracking analyzer (NTA). **C** Representative images of exosomes observed under transmission electron microscopy, scale bar = 100 nm. **D** Western blot experiment measuring the protein content of exosomal markers TSG101 and CD60. **E** Co-culture of Dil-labeled exosomes with THP-1 monocytes induced to differentiate into macrophages, with representative images observed under a fluorescence microscope, scale bar = 15 μm. **F** Real-time quantitative PCR and Western blot analysis of the expression levels of CD206, CD163, CD86 and CD80 in each group of cells, with corresponding bar graphs for statistical comparison. **G** Immunofluorescence staining to observe clusterin expression in different cell groups, with bar graphs showing the fluorescent positive area, scale bar = 25 μm. **H** Western blot analysis to detect the content of Clusterin protein, with bar graphs showing the grayscale value statistics. In Figure D, compared to the T98G group, $^{*}P < 0.05$, $^{**}P < 0.01$; compared to the U251 group, $\#P < 0.05$, $\#\#P < 0.01$. For Figures F-G, compared to the THP-1 group, $^{*}P < 0.05$, $^{**}P < 0.01$. Full-length blots/gels are presented in WB Uncropped Original Image. Data are presented as mean ± SD and comparisons between two groups were conducted using an unpaired t-test, while comparisons among multiple groups were performed using one-way ANOVA

indicating their significant involvement in tumor growth and metastasis [73]. The suppressive effect of M2 macrophages on immune cell attack is also considered to be related to tumor evasion of immune surveillance [74], highlighting the pivotal role of macrophage polarization in tumor immune mechanisms.

Collectively, the above experimental findings demonstrate that EVs derived from tumor stem cells can promote M2 macrophage polarization, which is likely an important mechanism underlying temozolomide resistance in glioblastoma cells.

clusterin-mediated M2 macrophage polarization promotes chemoresistance in glioblastoma cells

Clusterin, also known as CLU, is a highly conserved secretory glycoprotein that is believed to play a significant role in various biological processes such as apoptosis, cell signaling, and cell cycle regulation. In our study, we identified the presence of Clusterin aggregation in tumor stem cell vesicles. Our experimental results revealed that EVs from tumor stem cells could induce macrophage differentiation into the M2 phenotype when cocultured with PMA-activated THP-1 cells. Recent studies have linked Clusterin, a multifunctional protein, to macrophage polarization, suggesting that tumor stem cell-derived vesicles may mediate M2 macrophage polarization through Clusterin. To validate this hypothesis, we silenced Clusterin in isolated tumor stem cells, extracted the vesicles, and performed Western blot and RT-qPCR analyses to measure Clusterin levels. We observed a significant downregulation of Clusterin in the sh-Clusterin group (Fig. 7A, B).

Subsequently, to investigate the role of Clusterin in regulating macrophage polarization and its impact on temozolomide resistance in glioblastoma cells, we established temozolomide-resistant glioblastoma cell lines.

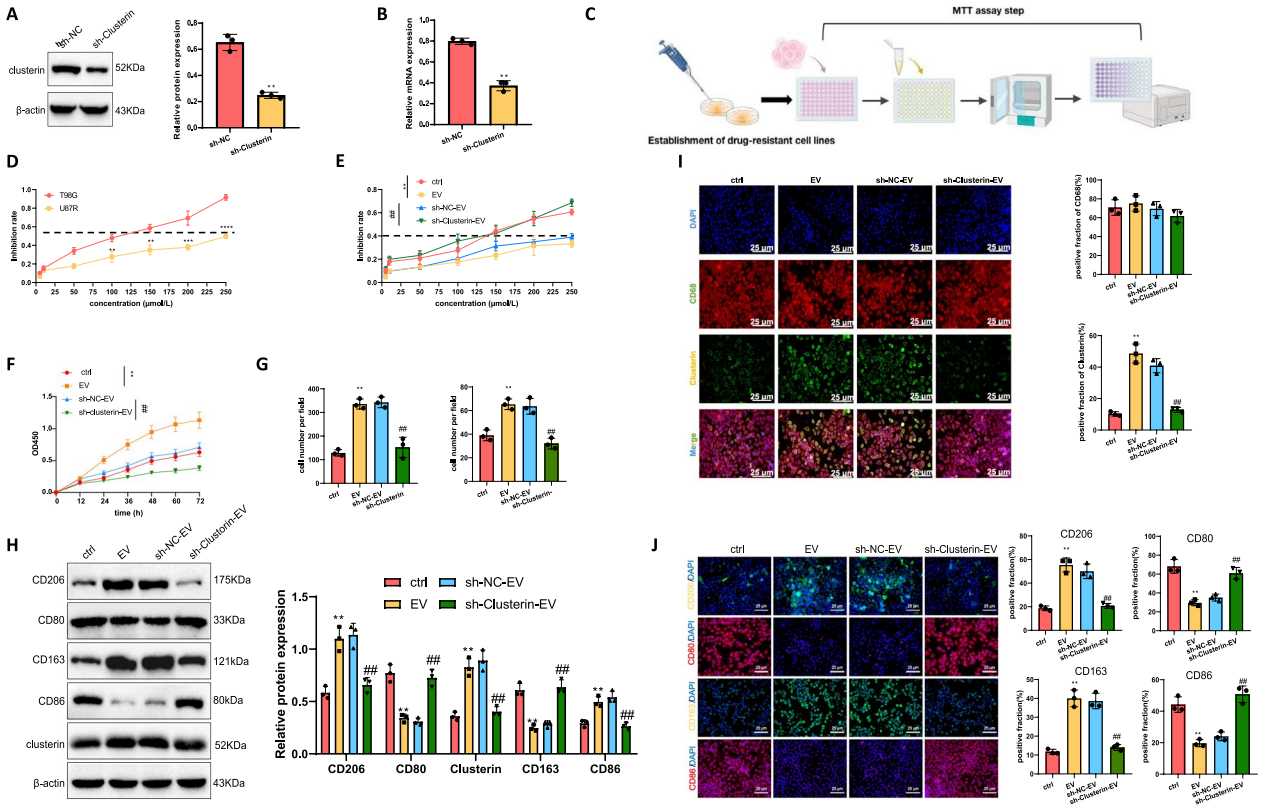

Fig. 7 Effects of Tumor Stem Cell EVs on Promoting Temozolomide Resistance in Glioblastoma Growth, Migration, and Invasion. Note: **A** Western blot analysis showing the protein expression levels of Clusterin in various cell groups, with corresponding grayscale statistical bar graph; **B** RT-qPCR results displaying the mRNA levels of Clusterin in different cell groups, presented in a statistical bar graph; **C** Flowchart of the MTT assay; **D** Viability and IC50 statistics of T98GR and T98G cells treated with different concentrations of temozolomide, measured by MTT assay; **E** Survival rates and IC50 values of drug-resistant cell lines treated with various concentrations of temozolomide, shown in a statistical table; **F** Cell viability of T98GR cells under 200 μM temozolomide stimulation assessed by CCK-8 assay; **G** Transwell experiment evaluating the migration and invasion abilities of different cell groups under 200 μM temozolomide stimulation; (H) Western blot analysis presenting the protein levels of CD206 and CD80 in various cell groups, with corresponding grayscale statistical bar graph; **I** Immunofluorescence staining for colocalization and positivity rates of CD68 and Clusterin in different cell groups, displayed in a statistical bar graph, scale bar = 25 μm; **J** Immunofluorescence staining showing the localization, quantification, and fluorescence positivity ratios of CD206 and CD80 in different cell groups, scale bar = 25 μm. Data are presented as mean ± SD, and comparisons between two groups were conducted using an unpaired t-test, while comparisons among multiple groups were performed using one-way ANOVA. For Panels A-B, compared with sh-NC, *$P < 0.05$, **$P < 0.01$; For Panel D, compared with the T98G group, *$P < 0.05$, **$P < 0.01$, ***$P < 0.001$, ****$P < 0.0001$; For Panels E-J, compared with the EV group, *$P < 0.05$, **$P < 0.01$, ***$P < 0.001$; compared with the sh-NC-EV group, #$P < 0.05$, ##$P < 0.01$, ###$P < 0.001$. Each cell experiment was conducted in triplicate. Full-length blots/gels are presented in WB Uncropped Original Image

By exposing T98G cells to increasing concentrations of temozolomide over a period of six months, we obtained the temozolomide-resistant cell line T98GR, with survival rates significantly higher than the parental T98G cells when treated with 200 μM temozolomide (Fig. 7C, D). MTT assays confirmed the acquired resistance, as the half-maximal inhibitory concentration (IC50) of the resistant cells was substantially higher than that of the parental cells. Further experiments were conducted to assess the effect of EVs and Clusterin on temozolomide resistance in glioblastoma cells. The T98GR cells were divided into four groups: ctrl group cocultured with THP-1, EV group cocultured with THP-1 and EVs, sh-NC-EV group transfected with empty lentivirus or silenced Clusterin along with THP-1 and EVs, and sh-Clusterin-EV group. MTT assays revealed a significant increase in IC50 in the EV group compared to the ctrl group, indicating enhanced resistance, while silencing Clusterin reduced IC50 to levels similar to the ctrl group, suggesting a reversal of the enhancing effect of EVs on glioblastoma temozolomide-resistant cells (Fig. 7E).

Furthermore, the four cell groups were stimulated with 200 μM temozolomide, and the proliferation, migration, and invasion capabilities were assessed to explore

whether EVs could enhance the biological functions of glioblastoma cells under temozolomide stimulation through Clusterin. Initially, CCK-8 assays indicated that the EV group had higher cell viability under temozolomide treatment compared to the ctrl group, while the sh-Clusterin-EV group showed lower viability than the sh-NC-EV group (Fig. 7F). These results suggested that EVs derived from tumor stem cells may enhance glioblastoma cell chemoresistance through Clusterin. Subsequent Transwell migration and invasion assays demonstrated that macrophages cocultured with tumor stem cell EVs significantly enhanced the migration and invasion abilities of temozolomide-resistant glioblastoma cells, which were attenuated by Clusterin silencing (Fig. 7G).

To observe macrophage polarization and the potential role of Clusterin, Western blot analysis was conducted to assess the expression levels of M1 and M2 macrophage markers and Clusterin in the various cell groups. The results showed a significant upregulation of the M2 macrophage marker CD206 and CD163 in the EV group, whereas the sh-Clusterin-EV group exhibited downregulation compared to the sh-NC-EV group. CD80 and CD86 an M1 macrophage marker, were downregulated in the EV group and upregulated in the sh-Clusterin-EV group. Regarding Clusterin expression, the EV group exhibited significant upregulation compared to the ctrl group, while the sh-Clusterin-EV group showed a notable decrease compared to the sh-NC-EV group (Fig. 7H). Immunofluorescence staining corroborated these findings, showing differing expression levels of Clusterin and macrophage markers among the groups, further supporting the involvement of Clusterin in macrophage functions (Fig. 7I). Finally, immunofluorescence analysis of CD80, CD86, CD163 and CD206 expression levels revealed that the EV group had a significant increase in CD206 positivity and a decrease in CD80 and CD86 positivity, while Clusterin silencing led to reduced CD206and CD163 positivity and increased CD80 and CD86 expression (Fig. 7J).

These results indicate that EVs from tumor stem cells may promote M2 macrophage polarization through Clusterin to enhance chemoresistance in glioblastoma cells. These findings provide additional support for the crucial role of tumor stem cell-derived vesicles in promoting glioblastoma chemoresistance and invasiveness through the key mechanism of Clusterin-induced M2 macrophage polarization.

In Vivo validation of M2 macrophage polarization promoting temozolomide resistance in glioblastoma cells

Building upon the discovery that EVs induced M2 macrophage polarization to promote temozolomide resistance in glioblastoma cells in vitro, we proceeded to validate these findings in vivo. Initially, we successfully established a subcutaneous xenograft tumor model in nude mice. Following the subcutaneous injection of T98G glioblastoma cells, visible tumor growth on the mice's skin surface occurred, with tumor volume increasing over time. Subsequently, to investigate the impact of EVs derived from tumor stem cells on temozolomide resistance in glioblastoma cell lines in vivo, we administered daily intragastric doses of 50 mg/kg temozolomide to the intervention group and injected EVs isolated from tumor stem cells at a dose of 200 μg/kg via tail vein every three days for four weeks. Tumor dimensions were regularly measured with calipers, and tumor volume calculations revealed sustained growth within four weeks post-injection. Notably, compared to the PBS group, the extracellular vesicle (EV) group exhibited accelerated tumor volume growth. In mice transfected with lentivirus-mediated Clusterin gene silencing, i.e., the sh-Clusterin + EV group, the tumor-promoting effect of EVs was suppressed (Fig. 8A, B). At the conclusion of the experiment, tumors were excised and weighed. The tumors from the EV group demonstrated significantly higher weight than those from the PBS group, whereas the sh-Clusterin + EV group exhibited a marked reduction in tumor weight compared to the sh-NC + EV group (Fig. 8C).

Subsequent histological examination through H&E staining and immunohistochemistry provided further insights into the impact of extracellular vesicle treatment on tumor tissue structure and microenvironment. Compared to the PBS group, the tissue structure in the EV group appeared denser, while the tissue structure in the sh-Clusterin + EV group resembled that of the PBS group, indicating that sh-Clusterin intervention modulated EV resistance to temozolomide (Fig. 8D).

Immunohistochemistry results indicated that in the EV extracellular vesicle-treated group, tumor tissues exhibited significantly increased expression of Clusterin and the M2 macrophage marker CD206 and CD163, alongside decreased expression of the M1 marker CD80 and CD86 compared to the PBS group. Conversely, in comparison to the sh-NC + EV group, the sh-Clusterin + EV group showed a substantial reduction in Clusterin expression and CD206 levels, while CD80 expression increased in tumor tissues (Fig. 8E, F). These findings suggest that EV treatment promotes M2 macrophage polarization, whereas Clusterin depletion can reverse the promoting effect of EV treatment on M2 macrophage polarization.

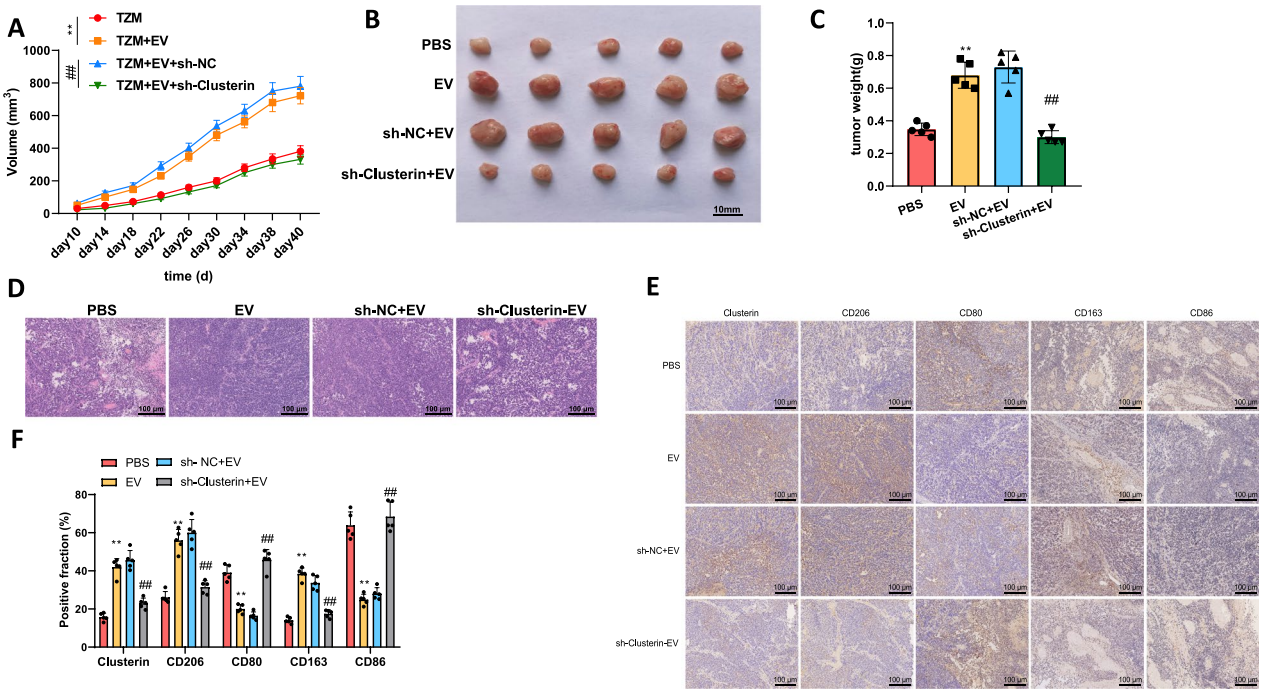

Fig. 8 Tumor Stem Cell-Derived EVs Mediate M2 Macrophage Polarization to Promote Glioblastoma Temozolomide Resistance and Tumor Growth. Note: **A** The growth of subcutaneous tumors in nude mice injected with temozolomide-resistant T98G glioblastoma cells over time; **B** Tumor volume growth in each group of nude mice with the untreated control group; **C** Images of excised tumor tissues at the end of the experiment along with quantitative analysis; **D** H&E staining of tumor tissues from each group of mice, scale bar = 100 μm; **E** Immunohistochemical staining to assess the expression levels of Clusterin, CD206, CD163, CD86, and CD80 in tumor tissue sections from two groups of mice, scale bar = 25 μm; **F** The positive staining area from immunohistochemical results. Data are presented as mean ± SD, and comparisons between two groups were conducted using an unpaired t-test, while comparisons among multiple groups were performed using one-way ANOVA. *$P < 0.05$, **$P < 0.01$ compared to the PBS group; #$P < 0.05$, ##$P < 0.01$ compared to the sh-NC + EV group. Each group consisted of five mice

Promote glioblastoma temozolomide resistance and tumor growth

Taken together, these results illustrate how EVs derived from tumor stem cells could potentially enhance tumor growth and development by influencing M2 macrophage polarization within the tumor microenvironment.

Discussion

In the current field of tumor research, the study of the tumor microenvironment has emerged as a critical research direction, supported by recent studies [75–77]. Particularly, various cellular components within the TME and their interactions play crucial roles in tumor development, metastasis, and resistance to therapy [78]. Macrophages, as one of the main immune cells within the TME, exhibit a dual role in tumor progression [79–81]. On one hand, M1 type macrophages possess anti-tumor properties; on the other hand, M2 type macrophages tend to promote tumor growth and metastasis, creating an immunosuppressive microenvironment for the tumor [82, 83]. Furthermore, tumor stem cells are considered pivotal drivers of malignant behavior within tumors, capable of exchanging information with cells in the TME through secreted EVs, thereby influencing tumor development [84–86]. However, previous research has been limited in understanding how tumor stem cells specifically affect the polarization status of macrophages through EVs, especially in highly malignant brain tumors like glioblastoma, and how this process impacts the tumor's resistance to the common chemotherapeutic agent temozolomide [87, 88].

This study delves into the intricate mechanisms of interaction between tumor stem cells and macrophages, particularly elucidating a novel mechanism by which tumor stem cells transmit Clusterin via EVs to mediate M2 macrophage polarization, offering a fresh perspective on glioblastoma resistance to temozolomide. In comparison to existing literature, the research not only unveils a new mechanism regulating macrophage polarization but also identifies the key role of Clusterin in this process. Previous studies have primarily focused on cytokines or chemical signals mediating macrophage polarization, while our research starts from the physical interaction between tumor stem cells and the TME, demonstrating

how tumor stem cells directly influence macrophage functional states through specific molecular mediators (i.e., Clusterin), paving the way for new insights into cellular communication mechanisms within the tumor microenvironment.

Furthermore, this study successfully identified key genes closely associated with M2 macrophage polarization and tumor stem cell functionality by combining single-cell sequencing technology with transcriptome sequencing, with Clusterin's role being particularly prominent. This work not only confirms Clusterin's critical role in regulating macrophage polarization but also provides a new methodological direction for future research endeavors. By constructing a PPI network using machine learning algorithms, we further bolster this finding, validating the high innovativeness and scientific rigor of our study. This comprehensive research methodology, blending bioinformatics tools with traditional biological experiments, offers an effective model for unraveling the molecular mechanisms underlying complex biological processes.

In exploring the intricate interplay between tumor stem cells and the tumor microenvironment, our study reveals that tumor stem cells not only directly influence macrophage polarization through extracellular vesicle secretion but also indirectly promote tumor growth, invasion, and drug resistance by altering other components within the TME. This outcome deepens our understanding of the roles tumor stem cells play in regulating the TME, particularly in elucidating how they exert a "commanding role" in the tumor microenvironment through signal molecule transmission via EVs. Compared to existing research, our study marks a significant advancement in uncovering the molecular mechanisms underlying cellular communication between tumor stem cells and the TME.

Regarding the mechanism of glioblastoma resistance to temozolomide, this study emphasizes the pivotal role played by M2 macrophages. Through a series of in vitro and in vivo experiments, we confirm that Clusterin delivered by tumor stem cell EVs effectively promotes M2 macrophage polarization, thereby enhancing glioblastoma cell resistance to temozolomide. M2 macrophages, also known as alternatively activated macrophages, produce survival-promoting molecules such as arginine, polyamines, and ornithine, as well as anti-inflammatory factors, growth factors, and angiogenic factors. These molecules facilitate tumor cell survival, proliferation, and metastasis, while suppressing the functions of other immune cells, such as T cells and NK cells, contributing to immunosuppressive responses. Thus, M2 macrophages are considered accomplices in tumor progression [73].

Recent years have seen a surge in anti-cancer strategies targeting macrophages, with one approach focused on inhibiting the generation and invasion of M2 macrophages. This can be achieved by targeting stimulatory factors or receptors specific to M2 macrophages. In this study, we identified Clusterin as a stimulatory factor for M2 macrophages. This discovery not only presents new insights for addressing drug resistance in the treatment of glioblastoma but also lays crucial scientific foundations for future drug development and treatment optimization strategies. Compared to prior studies on glioblastoma drug resistance, our research offers fresh insights at the molecular level of the resistance formation mechanism, especially in terms of how targeting specific cell types (such as M2 macrophages) may reverse tumor resistance.

The study further explores, based on our findings, how targeting Clusterin or modulating macrophage polarization could overcome glioblastoma drug resistance. These proposed therapeutic strategies, rooted in a profound understanding of glioblastoma pathogenesis, signal potential directions for future tumor treatment research. Notably, these strategies lay the groundwork for the combined use of immunotherapy, targeted therapy, and other treatment modalities, offering theoretical and experimental evidence for more effective treatment options for glioblastoma patients.

In conclusion, our study identifies a novel mechanism by which tumor stem cells mediate M2 macrophage polarization through extracellular vesicle transmission of Clusterin, thereby promoting temozolomide resistance in glioblastoma. This discovery not only enhances our understanding of intercellular communication mechanisms within the tumor microenvironment but also provides new targets and strategies for the treatment of malignant tumors such as glioblastoma. However, the limitations of this study should also be noted. For instance, the precise mechanisms by which Clusterin acts on macrophages to induce polarization and how M2-polarized macrophages contribute to glioblastoma resistance—through the secretion of specific substances and activation of particular pathways—require further investigation. Additionally, whether the same resistance mechanisms exist across all glioblastoma subtypes remains unclear, and the current findings need to be validated in larger clinical cohorts. Future studies will delve deeper into the role of Clusterin in other tumor types and explore effective ways to target this pathway for the treatment of glioblastoma and other malignant tumors. Furthermore, whether the mechanisms identified in this study can be translated into effective therapeutic interventions warrants further investigation.

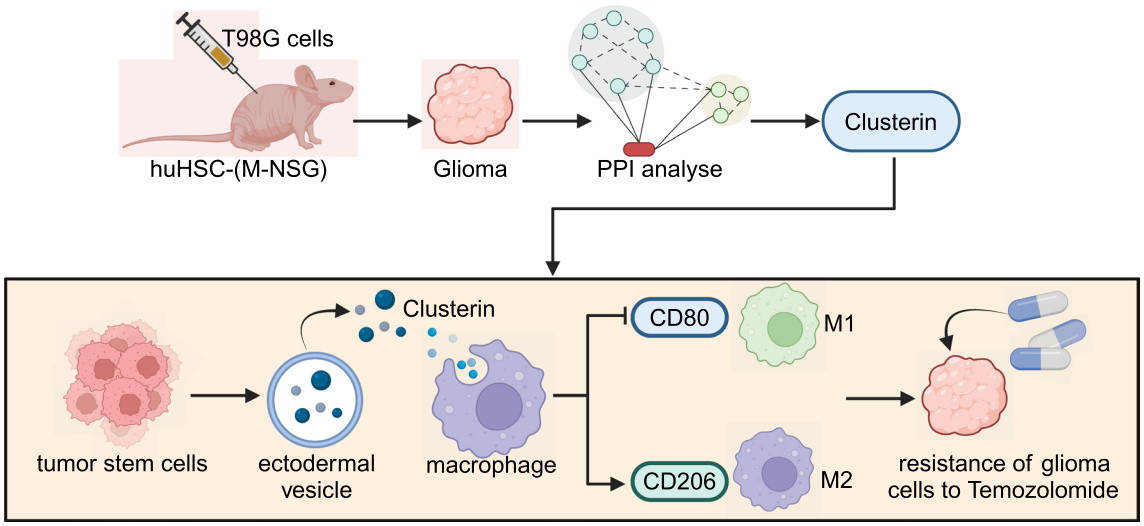

Fig. 9 Tumor Stem Cell-Derived Nanovesicles Promote Temozolomide Resistance in Glioblastoma Through Clusterin-Mediated Macrophage Polarization: Insights from Multiple Omics Studies

Conclusion

This study utilized machine learning-assisted multi-omics analysis to elucidate the crucial role of tumor stem cell-derived nanovesicle-mediated Clusterin transfer in regulating M2 macrophage polarization and its mechanism in promoting resistance of glioblastoma cells to temozolomide (Fig. 9). The research revealed that tumor stem cells communicate Clusterin via secreted EVs to induce M2 polarization in macrophages, thus influencing the drug resistance and invasive capabilities of glioblastoma cells. Moreover, this mechanism was validated in animal models, showing that extracellular vesicle treatment significantly slowed tumor growth and altered the tumor microenvironment. The scientific significance of this study lies in offering a fresh perspective on the complex interplay between tumor stem cells and immune cells in the glioblastoma microenvironment. Clinically, this finding holds promise for the development of novel therapeutic strategies, particularly targeting drug-resistant glioblastomas. However, limitations exist in the study, such as the need for further validation of the results in clinical samples from in vitro and animal models. Future research should focus on the universality of this mechanism in different subtypes and molecular features of glioblastoma, along with exploring the potential application of this mechanism in clinical treatments. Furthermore, gaining a deeper understanding of other potential roles of Clusterin in the tumor microenvironment is also a crucial direction for future research.

Supplementary Information

The online version contains supplementary material available at https://doi.org/10.1186/s13287-025-04247-z.

Additional file 1.

Additional file 2.

Additional file 3.

Acknowledgements

None.

Author contributions

Jianping Wen and Qingxia Shu conceived and designed the study. Jianping Wen and Xia Wu conducted the experiments, analyzed the data, and wrote the manuscript. Zhicheng Shu, Dongxu Wu, Zonghua Yin, Minglong Chen, Kun Luo, Kebo Liu, and Yi Le contributed to the experimental design, data collection, and analysis. Yulong Shen and Qingxia Shu provided critical revisions to the manuscript. All authors read and approved the final manuscript. Correspondence should be addressed to Jianping Wen and Qingxia Shu.

Funding

Not applicable.

Availability of data and materials

The sequencing data generated in this study have been deposited in the NCBI database under BioProject PRJNA1219799 and can be accessed through the following submission ID: SUB15068930. The raw sequencing data are available under the following accession numbers: Paracancerous group: Bulk RNA-seq: SRR32251009, SRR32251008, SRR32251007, Single-cell RNA-seq: SRR32251003 Tumor group: Bulk RNA-seq: SRR32251006, SRR32251005, SRR32251004. Single-cell RNA-seq: SRR32251002. The datasets are publicly available and can be accessed via the NCBI Sequence Read Archive (SRA).

Declarations

Ethics approval and consent to participate

All animal experimental procedures were approved by Hunan University of Medicine General Hospital's Experimental Animal Ethics Committee. Ethics approval for this study was granted by the Institutional Animal Care and Use Committee (IACUC) of Hunan University of Medicine General Hospital. The

project titled "Clusterin-Mediated Polarization of M2 Macrophages: A Mechanism of Temozolomide Resistance in Glioblastoma" was approved on February 12, 2023. The T98G glioblastoma cell line (CRL-1690) was obtained from ATCC (USA), which ensures compliance with ethical guidelines, including informed consent from the original donor and institutional ethical approval for cell line establishment. Further details are available at https://www.atcc.org/products/crl-1690. The U251 glioblastoma cell line (CC-Y5102) was obtained from Shanghai Enzyme Research Biological Technology Co., Ltd. (China), strictly for research purposes. The supplier follows standard ethical guidelines, but detailed donor consent information is not publicly available.

Consent for publication

All authors confirm their consent for publication.

Conflict of interest

The authors declare that they have no competing interests. The authors declare that they have not used Artificial Intelligence in this study.

Received: 29 July 2024 Accepted: 20 February 2025
Published online: 24 March 2025

References

1. Schaff LR, Mellinghoff IK. Glioblastoma and other primary brain malignancies in adults. JAMA. 2023;329:574. https://doi.org/10.1001/jama.2023.0023.
2. Gritsch S, Batchelor TT, Gonzalez Castro LN. Diagnostic, therapeutic, and prognostic implications of the 2021 World Health Organization classification of tumors of the central nervous system. Cancer. 2021;128:47–58. https://doi.org/10.1002/cncr.33918.
3. Bale TA, Rosenblum MK. The 2021 WHO classification of tumors of the central nervous system: an update on pediatric low-grade gliomas and glioneuronal tumors. Brain Pathol. 2022. https://doi.org/10.1111/bpa.13060.
4. Park YW, Han K, Park JE, Ahn SS, Kim EH, Kim J, et al. Leptomeningeal metastases in glioma revisited: incidence and molecular predictors based on postcontrast fluid-attenuated inversion recovery imaging. J Neurosurgery. 2023;139:38–48. https://doi.org/10.3171/2022.9.jns221659.
5. Daniel AGS, Hacker CD, Lee JJ, Dierker D, Humphries JB, Shimony JS, et al. Homotopic functional connectivity disruptions in glioma patients are associated with tumor malignancy and overall survival. Neuro-Oncol Adv. 2021. https://doi.org/10.1093/noajnl/vdab176.
6. Haizel-Cobbina J, Chen JW, Belete A, Dewan MC, Karekezi C. The landscape of neuro-oncology in East Africa: a review of published records. Childs Nerv Syst. 2021;37:2983–92. https://doi.org/10.1007/s00381-021-05344-z.
7. Li X, Moreira DC, Bag AK, Qaddoumi I, Acharya S, Chiang J. The clinical and molecular characteristics of progressive hypothalamic/optic pathway pilocytic astrocytoma. Neuro-Oncology. 2022;25:750–60. https://doi.org/10.1093/neuonc/noac241.
8. Huang X, Mu N, Ding Y, Huang R, Wu W, Li L, et al. Tumor microenvironment targeting for glioblastoma multiforme treatment via hybrid cell membrane coating supramolecular micelles. J Control Release. 2024;366:194–203. https://doi.org/10.1016/j.jconrel.2023.12.033.
9. Wang Q, Han B, Huang W, Qi C, Liu F. Identification of KIF15 as a potential therapeutic target and prognostic factor for glioma. Oncol Rep. 2020. https://doi.org/10.3892/or.2020.7510.
10. Ye J, Yang Y, Jin J, Ji M, Gao Y, Feng Y, et al. Targeted delivery of chlorogenic acid by mannosylated liposomes to effectively promote the polarization of TAMs for the treatment of glioblastoma. Bioact Mater. 2020;5:694–708. https://doi.org/10.1016/j.bioactmat.2020.05.001.
11. Wong SC, Kamarudin MNA, Naidu R. Anticancer mechanism of flavonoids on high-grade adult-type diffuse gliomas. Nutrients. 2023;15:797. https://doi.org/10.3390/nu15040797.
12. van Kempen EJ, Post M, Mannil M, Kusters B, ter Laan M, Meijer FJA, et al. Accuracy of machine learning algorithms for the classification of molecular features of gliomas on MRI: a systematic literature review and meta-analysis. Cancers. 2021;13:2606. https://doi.org/10.3390/cancers13112606.
13. Guowei L, Yanping J. Bioinformatics analysis of stem cell circ-ASB3 signaling pathway and its affection on glioma biological characteristics. Front Neuroinform. 2022. https://doi.org/10.3389/fninf.2022.859937.
14. van den Bent MJ, Tesileanu CMS, Wick W, Sanson M, Brandes AA, Clement PM, et al. Adjuvant and concurrent temozolomide for 1p/19q non-co-deleted anaplastic glioma (CATNON; EORTC study 26053–22054): second interim analysis of a randomised, open-label, phase 3 study. Lancet Oncol. 2021;22:813–23. https://doi.org/10.1016/s1470-2045(21)00090-5.
15. Hou X, Du H, Deng Y, Wang H, Liu J, Qiao J, et al. Gut microbiota mediated the individualized efficacy of Temozolomide via immunomodulation in glioma. J Transl Med. 2023. https://doi.org/10.1186/s12967-023-04042-5.
16. Doherty GJ, de Paula BHR. Cannabinoids in glioblastoma multiforme—hype or hope? Br J Cancer. 2021;124:1341–3. https://doi.org/10.1038/s41416-021-01265-5.
17. Latancia MT, Moreno NC, Leandro GS, Ribeiro VC, de Souza I, Vieira WKM, et al. DNA polymerase eta protects human cells against DNA damage induced by the tumor chemotherapeutic temozolomide. Mutat Res/Genet Toxicol Environ Mutagenesis. 2022;878:503498. https://doi.org/10.1016/j.mrgentox.2022.503498.
18. Silva JA, Colquhoun A. Effect of polyunsaturated fatty acids on temozolomide drug-sensitive and drug-resistant glioblastoma cells. Biomedicines. 2023;11:779. https://doi.org/10.3390/biomedicines11030779.
19. Song Y-Q, Li G-D, Niu D, Chen F, Jing S, Wai Wong VK, et al. A robust luminescent assay for screening alkyladenine DNA glycosylase inhibitors to overcome DNA repair and temozolomide drug resistance. J Pharm Anal. 2023;13:514–22. https://doi.org/10.1016/j.jpha.2023.04.010.
20. Sun Y, Dong D, Xia Y, Hao L, Wang W, Zhao C. YTHDF1 promotes breast cancer cell growth, DNA damage repair and chemoresistance. Cell Death Dis. 2022. https://doi.org/10.1038/s41419-022-04672-5.
21. An L, Cao Z, Nie P, Zhang H, Tong Z, Chen F, et al. Combinatorial targeting of Hippo-STRIPAK and PARP elicits synthetic lethality in gastrointestinal cancers. J Clin Investig. 2022. https://doi.org/10.1172/jci155468.
22. Li X, Wang S, Xie Y, Jiang H, Guo J, Wang Y, et al. Deacetylation induced nuclear condensation of HP1γ promotes multiple myeloma drug resistance. Nat Commun. 2023. https://doi.org/10.1038/s41467-023-37013-x.
23. Wang J, Yu H, Dong W, Zhang C, Hu M, Ma W, et al. N6-Methyladenosine–mediated up-regulation of FZD10 regulates liver cancer stem cells' properties and Lenvatinib resistance through WNT/β-catenin and hippo signaling pathways. Gastroenterology. 2023;164:990–1005. https://doi.org/10.1053/j.gastro.2023.01.041.
24. Stelmach P, Trumpp A. Leukemic stem cells and therapy resistance in acute myeloid leukemia. Haematologica. 2023;108:353–66. https://doi.org/10.3324/haematol.2022.280800.
25. Zhou Y, Xu J, Luo H, Meng X, Chen M, Zhu D. Wnt signaling pathway in cancer immunotherapy. Cancer Letters. 2022;525:84–96. https://doi.org/10.1016/j.canlet.2021.10.034.
26. Karami Fath M, Babakhaniyan K, Anjomrooz M, Jalalifar M, Alizadeh SD, Pourghasem Z, et al. Recent advances in glioma cancer treatment: conventional and epigenetic realms. Vaccines. 2022;10:1448. https://doi.org/10.3390/vaccines10091448.
27. Piperi C, Markouli M, Gargalionis AN, Papavassiliou KA, Papavassiliou AG. Deciphering glioma epitranscriptome: focus on RNA modifications. Oncogene. 2023;42:2197–206. https://doi.org/10.1038/s41388-023-02746-y.
28. Banerjee K, Núñez FJ, Haase S, McClellan BL, Faisal SM, Carney SV, et al. Current approaches for glioma gene therapy and virotherapy. Front Mol Neurosci. 2021. https://doi.org/10.3389/fnmol.2021.621831.
29. Mazurek M, Rola R. The implications of nitric oxide metabolism in the treatment of glial tumors. Neurochem Int. 2021;150:105172. https://doi.org/10.1016/j.neuint.2021.105172.
30. Corsini M, Ravelli C, Grillo E, Dell'Era P, Presta M, Mitola S. Simultaneously characterization of tumoral angiogenesis and vasculogenesis in stem cell-derived teratomas. Exp Cell Res. 2021;400:112490. https://doi.org/10.1016/j.yexcr.2021.112490.
31. Ikeda S, Tagawa H. Impact of hypoxia on the pathogenesis and therapy resistance in multiple myeloma. Cancer Sci. 2021;112:3995–4004. https://doi.org/10.1111/cas.15087.
32. Zhao Y, Guo S, Deng J, Shen J, Du F, Wu X, et al. VEGF/VEGFR-Targeted therapy and immunotherapy in non-small cell lung cancer: targeting the

tumor microenvironment. Int J Biol Sci. 2022;18:3845–58. https://doi.org/10.7150/ijbs.70958.
33. de Rooij LPMH, Becker LM, Teuwen L-A, Boeckx B, Jansen S, Feys S, et al. The pulmonary vasculature in lethal COVID-19 and idiopathic pulmonary fibrosis at single-cell resolution. Cardiovasc Res. 2022;119(2):520–35. https://doi.org/10.1093/cvr/cvac139.
34. Darragh LB, Karam SD. Amateur antigen-presenting cells in the tumor microenvironment. Mol Carcinog. 2021;61(2):153–64. https://doi.org/10.1002/mc.23354.
35. Liu Q-P, Chen Y-Y, An P, Rahman K, Luan X, Zhang H. Natural products targeting macrophages in tumor microenvironment are a source of potential antitumor agents. Phytomedicine. 2023;109:154612. https://doi.org/10.1016/j.phymed.2022.154612.
36. Cheng P, Li S, Chen H. Macrophages in lung injury, repair, and fibrosis. Cells. 2021;10(2):436. https://doi.org/10.3390/cells10020436.
37. Zhou C, Weng J, Liu C, Liu S, Hu Z, Xie X, et al. Disruption of SLFN11 deficiency-induced CCL2 signaling and macrophage M2 polarization potentiates Anti–PD-1 therapy efficacy in hepatocellular carcinoma. Gastroenterology. 2023;164:1261–78. https://doi.org/10.1053/j.gastro.2023.02.005.
38. Wu H, Zheng J, Xu S, Fang Y, Wu Y, Zeng J, et al. Mer regulates microglial/macrophage M1/M2 polarization and alleviates neuroinflammation following traumatic brain injury. J Neuroinflammation. 2021. https://doi.org/10.1186/s12974-020-02041-7.
39. Zhao K, Calero-Pérez P, Bopp MHA, Möschl V, Pagenstecher A, Mulero-Acevedo M, et al. Correlation of MR-based metabolomics and molecular profiling in the tumor microenvironment of temozolomide-treated orthotopic GL261 glioblastoma in mice. IJMS. 2023;24:17628. https://doi.org/10.3390/ijms242417628.
40. Chen Z, Hambardzumyan D. Macrophage-tumor cell intertwine drives the transition into a mesenchymal-like cellular state of glioblastoma. Cancer Cell. 2021;39:743–5. https://doi.org/10.1016/j.ccell.2021.05.003.
41. Gao Z, Xu J, Fan Y, Zhang Z, Wang H, Qian M, et al. ARPC1B promotes mesenchymal phenotype maintenance and radiotherapy resistance by blocking TRIM21-mediated degradation of IFI16 and HuR in glioma stem cells. J Exp Clin Cancer Res. 2022. https://doi.org/10.1186/s13046-022-02526-8.
42. Zhu X, Fang Y, Chen Y, Chen Y, Hong W, Wei W, et al. Interaction of tumor-associated microglia/macrophages and cancer stem cells in glioma. Life Sci. 2023;320:121558. https://doi.org/10.1016/j.lfs.2023.121558.
43. Alejo S, Palacios BE, Venkata PP, He Y, Li W, Johnson JD, et al. Lysine-specific histone demethylase 1A (KDM1A/LSD1) inhibition attenuates DNA double-strand break repair and augments the efficacy of temozolomide in glioblastoma. Neuro-Oncology. 2023;25:1249–61. https://doi.org/10.1093/neuonc/noad018.
44. Jiang VC, Hao D, Jain P, Li Y, Cai Q, Yao Y, et al. TIGIT is the central player in T-cell suppression associated with CAR T-cell relapse in mantle cell lymphoma. Mol Cancer. 2022. https://doi.org/10.1186/s12943-022-01655-0.
45. Zhao X, Henderson HJ, Wang T, Liu B, Li Y. Deletion of clusterin protects cochlear hair cells against hair cell aging and ototoxicity. Neural Plast. 2021;2021:1–14. https://doi.org/10.1155/2021/9979157.
46. Menna G, Mattogno PP, Donzelli CM, Lisi L, Olivi A, Della Pepa GM. Glioma-associated microglia characterization in the glioblastoma microenvironment through a 'seed-and soil' approach: a systematic review. Brain Sci. 2022;12:718. https://doi.org/10.3390/brainsci12060718.
47. Dinevska M, Widodo SS, Furst L, Cuzcano L, Fang Y, Mangiola S, et al. Cell signaling activation and extracellular matrix remodeling underpin glioma tumor microenvironment heterogeneity and organization. Cell Oncol. 2022;46:589–602. https://doi.org/10.1007/s13402-022-00763-9.
48. Butler A, Hoffman P, Smibert P, Papalexi E, Satija R. Integrating single-cell transcriptomic data across different conditions, technologies, and species. Nat Biotechnol. 2018;36:411–20. https://doi.org/10.1038/nbt.4096.
49. Trapnell C, Cacchiarelli D, Grimsby J, Pokharel P, Li S, Morse M, Lennon NJ, Livak KJ, Mikkelsen TS, Rinn JL. The dynamics and regulators of cell fate decisions are revealed by pseudotemporal ordering of single cells. Nat Biotechnol. 2014;32(4):381–6. https://doi.org/10.1038/nbt.2859.
50. Lin W, Wang Y, Chen Y, Wang Q, Gu Z, Zhu Y. Role of calcium signaling pathway-related gene regulatory networks in ischemic stroke based on multiple WGCNA and single-cell analysis. Oxidative Med Cell Longev. 2021. https://doi.org/10.1155/2021/8060477.
51. Zuo Z, Shen J-X, Pan Y, Pu J, Li Y-G, Shao X, et al. Weighted gene correlation network analysis (WGCNA) detected loss of MAGI2 promotes chronic kidney disease (CKD) by podocyte damage. Cell Physiol Biochem. 2018;51:244–61. https://doi.org/10.1159/000495205.
52. Guangchuang Y, Wang L-G, Han Y, He Q-Y. ClusterProfiler: an R package for comparing biological themes among gene clusters. OMICS: J Integr Biol. 2012;16(5):284–7. https://doi.org/10.1089/omi.2011.0118.
53. Guo C, Gao Y, Ju Q, Zhang C, Gong M, Li Z. The landscape of gene co-expression modules correlating with prognostic genetic abnormalities in AML. J Transl Med. 2021. https://doi.org/10.1186/s12967-021-02914-2.
54. Sanz H, Valim C, Vegas E, Oller JM, Reverter F. SVM-RFE: selection and visualization of the most relevant features through non-linear kernels. BMC Bioinf. 2018. https://doi.org/10.1186/s12859-018-2451-4.
55. Alderden J, Pepper GA, Wilson A, Whitney JD, Richardson S, Butcher R, et al. Predicting pressure injury in critical care patients: a machine-learning model. Am J Crit Care. 2018;27:461–8. https://doi.org/10.4037/ajcc2018525.
56. Wu Y, Liu X, Li G. Integrated bioinformatics and network pharmacology to identify the therapeutic target and molecular mechanisms of Huangqin decoction on ulcerative Colitis. Sci Rep. 2022. https://doi.org/10.1038/s41598-021-03980-8.
57. Sierra-López F, Castelan-Ramírez I, Hernández-Martínez D, Salazar-Villatoro L, Segura-Cobos D, Flores-Maldonado C, et al. Extracellular vesicles secreted by Acanthamoeba culbertsoni have cox and proteolytic activity and induce Hemolysis. Microorganisms. 2023;11:2762. https://doi.org/10.3390/microorganisms11112762.
58. Jin D, Guo J, Wu Y, Du J, Yang L, Wang X, et al. Retracted article: m6A mRNA methylation initiated by METTL3 directly promotes YAP translation and increases YAP activity by regulating the MALAT1-miR-1914-3p-YAP axis to induce NSCLC drug resistance and metastasis. J Hematol Oncol. 2019. https://doi.org/10.1186/s13045-019-0830-6.
59. Walentowicz-Sadlecka M, Dziobek K, Grabiec M, Sadlecki P, Walentowicz P, Mak P, et al. The analysis of human leukocyte antigen-G level in patients with endometrial cancer by Western blot technique. Am J Rep Immunol. 2018. https://doi.org/10.1111/aji.13070.
60. Yao J, Wang J, Xu Y, Guo Q, Sun Y, Liu J, et al. CDK9 inhibition blocks the initiation of PINK1-PRKN-mediated mitophagy by regulating the SIRT1-FOXO3-BNIP3 axis and enhances the therapeutic effects involving mitochondrial dysfunction in hepatocellular carcinoma. Autophagy. 2021;18:1879–97. https://doi.org/10.1080/15548627.2021.2007027.
61. Wang Y, Zhang L, Che X, Li W, Liu Z, Jiang J. Roles of SIRT1/FoxO1/SREBP-1 in the development of progestin resistance in endometrial cancer. Arch Gynecol Obstet. 2018;298:961–9. https://doi.org/10.1007/s00404-018-4893-3.
62. Zhang L, Liu X, Huang M, Wang R, Zhu W, Li Y, et al. Metformin inhibits HaCaT cell proliferation under hyperlipidemia through reducing reactive oxygen species via FOXO3 activation. CCID. 2022;15:1403–13. https://doi.org/10.2147/ccid.s368845.
63. Liu Y, Cai X, Cai Y, Chang Y. lncRNA OIP5-AS1 suppresses cell proliferation and invasion of endometrial cancer by regulating PTEN/AKT via sponging miR-200c-3p. J Immunol Res. 2021;1:1–16. https://doi.org/10.1155/2021/4861749.
64. Pan X, Hong X, Li S, Meng P, Xiao F. METTL3 promotes adriamycin resistance in MCF-7 breast cancer cells by accelerating pri-microRNA-221–3p maturation in a m6A-dependent manner. Exp Mol Med. 2021;53:91–102. https://doi.org/10.1038/s12276-020-00510-w.
65. Wang S, Cheng M, Zheng X, Zheng L, Liu H, Lu J, et al. Interactions between lncRNA TUG1 and miR-9–5p modulate the resistance of breast cancer cells to doxorubicin by regulating eIF5A2. OTT. 2020;13:13159–70. https://doi.org/10.2147/ott.s255113.
66. Fan Y, Dong Z, Shi Y, Sun S, Wei B, Zhan L. NLRC5 promotes cell migration and invasion by activating the PI3K/AKT signaling pathway in endometrial cancer. J Int Med Res. 2020. https://doi.org/10.1177/0300060520925352.
67. Yin J, Kim SS, Choi E, Oh YT, Lin W, Kim T-H, et al. ARS2/MAGL signaling in glioblastoma stem cells promotes self-renewal and M2-like polarization of tumor-associated macrophages. Nat Commun. 2020. https://doi.org/10.1038/s41467-020-16789-2.
68. Saraswati S, Alhaider A, Abdelgadir AM, Tanwer P, Korashy HM. Phloretin attenuates STAT-3 activity and overcomes sorafenib resistance targeting SHP-1–mediated inhibition of STAT3 and Akt/VEGFR2 pathway in

hepatocellular carcinoma. Cell Commun Signal. 2019. https://doi.org/10.1186/s12964-019-0430-7.
69. Ke M, Zhang Z, Xu B, Zhao S, Ding Y, Wu X, et al. Baicalein and baicalin promote antitumor immunity by suppressing PD-L1 expression in hepatocellular carcinoma cells. Int Immunopharmacol. 2019;75:105824. https://doi.org/10.1016/j.intimp.2019.105824.
70. Xia D, Zhang X-R, Ma Y-L, Zhao Z-J, Zhao R, Wang Y-Y. Nrf2 promotes esophageal squamous cell carcinoma (ESCC) resistance to radiotherapy through the CaMKIIα-associated activation of autophagy. Cell Biosci. 2020. https://doi.org/10.1186/s13578-020-00456-6.
71. Sheehan PW, Nadarajah CJ, Kanan MF, Patterson JN, Novotny B, Lawrence JH, et al. An astrocyte BMAL1-BAG3 axis protects against alpha-synuclein and tau pathology. Neuron. 2023;111:2383–98. https://doi.org/10.1016/j.neuron.2023.05.006.
72. Li D, Zhang Q, Li L, Chen K, Yang J, Dixit D, et al. β2-Microglobulin maintains glioblastoma stem cells and induces M2-like polarization of tumor-associated macrophages. Cancer Res. 2022;82:3321–34. https://doi.org/10.1158/0008-5472.can-22-0507.
73. Li M, Yang Y, Xiong L, Jiang P, Wang J, Li C. Metabolism, metabolites, and macrophages in cancer. J Hematol Oncol. 2023. https://doi.org/10.1186/s13045-023-01478-6.
74. Zhang X, Wei Z, Yong T, Li S, Bie N, Li J, et al. Cell microparticles loaded with tumor antigen and resiquimod reprogram tumor-associated macrophages and promote stem-like CD8+ T cells to boost anti-PD-1 therapy. Nat Commun. 2023. https://doi.org/10.1038/s41467-023-41438-9.
75. Winkler F, Venkatesh HS, Amit M, Batchelor T, Demir IE, Deneen B, et al. Cancer neuroscience: state of the field, emerging directions. Cell. 2023;186:1689–707. https://doi.org/10.1016/j.cell.2023.02.002.
76. Bejarano L, Jordão MJC, Joyce JA. Therapeutic targeting of the tumor microenvironment. Cancer Discovery. 2021;11:933–59. https://doi.org/10.1158/2159-8290.cd-20-1808.
77. Zhou W-T, Jin W-L. B7–H3/CD276: an emerging cancer immunotherapy. Front Immunol. 2021. https://doi.org/10.3389/fimmu.2021.701006.
78. Badve SS, Gökmen-Polar Y. Targeting the tumor-tumor microenvironment crosstalk. Expert Opin Ther Targets. 2023;27:447–57. https://doi.org/10.1080/14728222.2023.2230362.
79. Wang S, Li F, Ye T, Wang J, Lyu C, Qing S, et al. Macrophage-tumor chimeric exosomes accumulate in lymph node and tumor to activate the immune response and the tumor microenvironment. Sci Transl Med. 2021. https://doi.org/10.1126/scitranslmed.abb6981.
80. He K, Barsoumian HB, Puebla-Osorio N, Hu Y, Sezen D, Wasley MD, et al. Inhibition of STAT6 with antisense oligonucleotides enhances the systemic antitumor effects of radiotherapy and Anti–PD-1 in metastatic non-small cell lung cancer. Cancer Immunol Res. 2023;11:486–500. https://doi.org/10.1158/2326-6066.cir-22-0547.
81. Chen Q, Li Y, Gao W, Chen L, Xu W, Zhu X. Exosome-mediated crosstalk between tumor and tumor-associated macrophages. Front Mol Biosci. 2021. https://doi.org/10.3389/fmolb.2021.764222.
82. Yang M, Wang B, Yin Y, Ma X, Tang L, Zhang Y, et al. PTN-PTPRZ1 signaling axis blocking mediates tumor microenvironment remodeling for enhanced glioblastoma treatment. J Control Release. 2023;353:63–76. https://doi.org/10.1016/j.jconrel.2022.11.025.
83. Zeng Y-X, Chou K-Y, Hwang J-J, Wang H-S. The effects of IL-1β stimulated human umbilical cord mesenchymal stem cells on polarization and apoptosis of macrophages in rheumatoid arthritis. Sci Rep. 2023. https://doi.org/10.1038/s41598-023-37741-6.
84. Wu Y, Song Y, Wang R, Wang T. Molecular mechanisms of tumor resistance to radiotherapy. Mol Cancer. 2023. https://doi.org/10.1186/s12943-023-01801-2.
85. Lin Z, Wu Y, Xu Y, Li G, Li Z, Liu T. Mesenchymal stem cell-derived exosomes in cancer therapy resistance: recent advances and therapeutic potential. Mol Cancer. 2022. https://doi.org/10.1186/s12943-022-01650-5.
86. Barthel L, Hadamitzky M, Dammann P, Schedlowski M, Sure U, Thakur BK, Hetze S. Glioma: molecular signature and crossroads with tumor microenvironment. Cancer Metastasis Rev. 2021;41(1):53–75. https://doi.org/10.1007/s10555-021-09997-9.
87. Shan S, Chen J, Sun Y, Wang Y, Xia B, Tan H, et al. Functionalized macrophage exosomes with panobinostat and PPM1D-siRNA for diffuse intrinsic pontine gliomas therapy. Adv Sci. 2022. https://doi.org/10.1002/advs.202200353.
88. Adamus T, Hung C-Y, Yu C, Kang E, Hammad M, Flores L, et al. Glioma-targeted delivery of exosome-encapsulated antisense oligonucleotides using neural stem cells. Mol Ther Nucl Acids. 2022;27:611–20. https://doi.org/10.1016/j.omtn.2021.12.029.

Publisher's Note